Journal of Applied Geophysics 163 (2019) 55–72

Contents lists available at ScienceDirect

Journal of Applied Geophysics

journal homepage: www.elsevier.com/locate/jappgeo

Seismic site classification and correlation between V_S and SPT-N for deep soil sites in Indo-Gangetic Basin

Ketan Bajaj, P. Anbazhagan *

Indian Institute of Science, Bangalore, India

ARTICLE INFO

Article history:
Received 8 June 2018
Received in revised form 19 December 2018
Accepted 20 February 2019
Available online 28 February 2019

Keywords:
Seismic site classification
V_S and SPT-N correlation
V_{S30}
Indo-Gangetic basin
Deep sedimentary deposits
Surface wave methods

ABSTRACT

The Indo-Gangetic Basin (IGB) is occupied by the thick deposits of different types of loose to dense soil due to the active sedimentation. Till date, no detailed study has been carried out on seismic site characterization, and classification considering shear wave velocity >50 m depth. In this study, surface wave survey was used for determining the shear wave velocity (V_S) variation with depth at 276 locations in the IGB using low-frequency geophones by performing combined active (Multichannel analysis of surface waves, MASW) and passive (Ambient Noise) surveys. To study the spatial variability of V_S, based on the sediment deposition and geological variability, the whole IGB has been divided into Punjab-Haryana region (PHR), Uttar Pradesh region (UPR), and Bihar region (BR). Firstly, using the least square, orthogonal, and mixed effect approaches, a new correlation between the V_S and SPT-N has been developed for all the three regions separately. The V_S and SPT-N correlation has been developed considering both corrected and uncorrected SPT-N value. The residuals have been determined using the observed and the predicted V_S values from newly developed V_S and SPT-N correlation from each approach. For the same SPT-N value, correlation for UPR region is predicting high V_S value as compared to other two regions. Studying the variation of residuals with V_S, it is determined that the mixed effect is performing better for $V_S \leq 250$ m/s and orthogonal for $V_S > 250$ m/s. At higher N-value, difference between V_S values for all the three regions are noticeable. Further, the newly developed relationships are compared with the existing V_S and SPT-N relationship. Additionally, the IGB is classified based on the average shear wave velocity in the top 30 m (V_{S30}) as per the National Earthquake Hazards Reduction Program (NEHRP) and compared with Eurocode 8 (EC8). The V_{S30} is high in the southern part of the BR and UPR and low near to the active channel deposition and major part of the IGB is classified as seismic site class D. Most of the IGB sites have experienced severe damage either due to local site effects or liquefaction during past earthquakes. Therefore, the spatial variability of the average shear wave velocity at different depths, i.e., at top 5,10,15,20, 30 50, 100, 150, 200, 250 and 300 m are also estimated and compared with the available basement depth map.

1. Introduction

The Ganga Basin is an overfilled active foreland basin that has a predominant peripheral bulge where sedimentation is taking place majorly because of the fluvial process (Singh, 1996). Significant variability of soil deposition depth has been reported by the Geological Society of India (GSI, 2006) along the entire stretch of the Indo-Gangetic Basin (IGB). Moreover, the IGB lies contagious to the world's most seismically active Himalayan region. Any seismic activity in the Himalaya region results in significant economic and human loss in the foreland basin (i.e., IGB). Evidence can also be drawn from historical earthquakes (e.g., 1934 Bihar-Nepal; 2005 Kashmir earthquake; 2015 Nepal earthquake). Considering the weak motion in the central IGB, Srinagesh et al. (2011) reported the amplification of 2–4 times in the peak ground acceleration due to the presence of deep basin. Hence, characterizing and classifying the deep deposits of the IGB is the prime necessity to study the seismic wave amplification in the region.

Surface wave methods are widely used to estimate the shear wave velocity (V_S) of the near surface material, as these methods are more robust, non-invasive and low cost than the direct methods (e.g. crosshole and downhole seismic) (Foti et al., 2009, 2011; Socco et al., 2010). From last few decades multichannel analysis of surface waves (MASW) has emerged as a promising technique to determine V_S of near surface material for seismic site classification. Various researchers (e.g. Rahman et al., 2016; Raef et al., 2015; Orubu et al., 2018; Karabulut, 2018a etc.) used the MASW method for determining the V_S profiles for seismic site classification other than study area. Using MASW, various researchers have made an attempt to develop the site classification map for different parts of India (Anbazhagan and Sitharam, 2008; Mahajan et al., 2007, 2012; Satyam and Rao, 2008; Anbazhagan et al., 2013).

* Corresponding author.
E-mail addresses: ketanbajaj@iisc.ac.in (K. Bajaj), anbazhagan@iisc.ac.in (P. Anbazhagan).

https://doi.org/10.1016/j.jappgeo.2019.02.011
0926-9851/

Anbazhagan and Sitharam (2008), Mahajan et al. (2007, 2012), Maheshwari et al. (2010), Satyam and Rao (2008) and Anbazhagan et al. (2013) have developed shear wave velocity map for Bangalore, Dehradun, Chennai, Delhi, and Lucknow, respectively. However, these previous studies are limited to shallow depths, i.e. up to 50 m depth. Till date no extensive study has been done for site characterization of the deep soil deposits in the entire IGB. This is the first time such an extensive study has been carried out in the entire stretch of the IGB, for determining the V_s values at shallow and deeper depths.

Although, surface methods are widely used in many engineering applications, several issues related to that are unresolved and these methoths are still developing and evolving (Socco et al., 2010). Aditionally, expertise in geophysical knowledge and testing is required to carry out these seismic surveys. Some of these tests are difficult to be carried out in densely built up areas in the city. Therefore the V_S can also be estimated from standard penetration test blow count (SPT-N) by developing the correlation between V_S and the SPT-N value. In this study, V_S and the SPT-N value relationships have been developed by dividing the study area into three parts, i.e., Punjab-Haryana Region (PHR), Uttar Pradesh (UPR) and Bihar Region (BR).

Loose soil deposit and water table at shallow depth may result in an excessive settlement and liquefaction due to dynamic loading. Also, deep sedimentation widely affects the spectral period and surface amplification (Malekmohammadi and Pezeshk, 2015). Hence, it is indispensable to study the subsurface characteristics of both shallow and deep soil deposits. In this study, combined active and passive/ambient noise multichannel analysis of surface wave (MASW) survey has been used for determining the shear wave velocity (V_S) profile at 276 locations in the IGB. For evaluating the dispersion characteristics, both active and passive sources, the linear and circular array have been used. Due to the development and improvement of its algorithm and data acquisition procedure, it has emerged as a promising technique to estimate the V_S of the deep soil site. Firstly, using the least square, orthogonal and mixed effect approaches, a new correlation between the V_S and SPT-N has been developed for PHR, UPR, BR and the whole IGB. Both corrected and uncorrected SPT-N values have been used in this study for developing a new correlation between V_S and SPT-N values for the IGB. The suitability of these approaches has been tested based on residual analysis by comparing the predicted and recorded V_S values. The obtained V_S is further used for determining the average shear wave velocity at top 30 m (V_{S30}). The whole study area has been classified as per the National Earthquake Hazards Reduction Program (NEHRP) and compared with Eurocode 8 (EC8) by dividing it into PHR, UPR and BR. Further, the spatial variability of the average shear wave velocity for deeper depths i.e. at top 100 and 300 m is also studied and compared with the available basement depth map.

2. Geology and seismotectonic of study area

The IGB is well known as the Himalayan foredeep depression formed because of post-collision between the Indian and Eurasian tectonic plates during the Cenozoic growth of the Himalayas. The displaced river terraces, geomorphic surfaces, topographic ridges and alluvial fans are some of the potential indicators of the active tectonics manifested in the IGB (Singh, 1996). The present study area occupies an area around 250,000 km^2, which is a part of the Himalayan foreland basin and lies roughly between longitude 74° E, and 88° E and latitude 24° N and 32° N (Fig. 1). The Ganga foreland basin originated in the early Miocene (~20 Ma) and from middle Miocene (~15 Ma) to middle Pleistocene (~500 Ka), the northern part of the IGB was uplifted, and thrust towards basin and the Ganga plains shifted southwards in response to thrust loading in the orogen (Singh, 1996). Burbank (1992) concluded that the Ganga Plain foreland basin (i.e., UPR and BR) has been dominated by transverse river system since the Pliocene (~4 Ma) because of erosionally-driven uplift, whereas, longitudinal river dominates Indus foreland basin (i.e., few parts of PHR) due to tectonically-driven uplift. Foreland basin in PHR is overfilled basin and UPR, and BR is an underfilled basin (Burbank, 1992). The Ganga foreland basin shows all the major components of a foreland basin, namely orogen (the Himalaya), deformed and uplifted foreland basin deposits adjacent to orogen (Siwalik hills), a depositional basin (Ganga Plain), and peripheral cratonic bulge (Bundelkhand-Vindhyan Plateau) (Singh, 1996). The present study area concentrates on Gangetic plain (central portion of Ganga foreland basin) and Punjab-Haryana foreland basin (Part of Indus foreland basin). Based on the geographical position and geomorphology, the Ganga Plain is further subdivided into western Gangetic Plain located in Uttar Pradesh and eastern Gangetic Plain located in the State of Bihar.

PHR is a vast alluvial plain, bounded by Siwalik Hills of Himalaya in the north and Aravalli-Delhi Massif in the south, formed by essentially fluvial processes. This region is covered by the Quaternary aeolian and alluvial deposits, which nonuniformly lies over the quartzite and granite of the Delhi Subgroup, Nagaur sandstone of the Cambrian age and Tertiary clay (Saini and Anand, 1996). Saini and Anand (1996) described

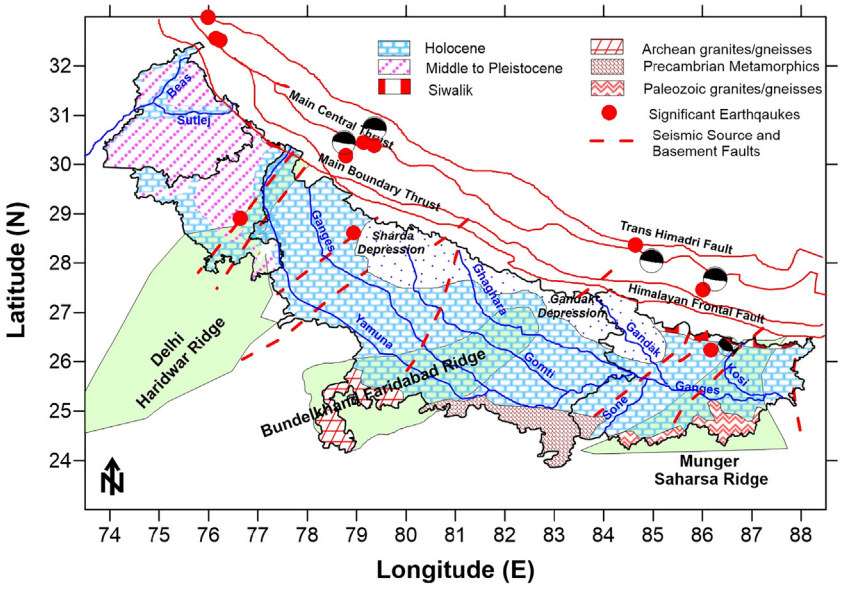

Fig. 1. Geological Map along with seismological parameter of Indo Gangetic Basin.

the Quaternary sediments of Northwestern Haryana by classifying it into Banda Alluvium, Varanasi older alluvium, older aeolian deposit and newer aeolian deposit/alluvium. Kumar et al. (1996) described the sequence stratigraphy of UPR by diving it into the four sequences, i.e., sequence 1 indicates the continental sedimentation ranging in age from the upper Eocene to lower Miocene and sequence 4 indicates the youngest and on-going cycle of the Quaternary sedimentation in the Holocene. As per Om Prakash et al. (1990), most of the middle Ganga alluvial tract lies on the Quaternary alluvium that directly lies over the late Proterozoic Vindhyan Basement. Bisaria et al. (1996) classified the Quaternary alluvium Ganga into older alluvium which comprises Banda alluvium and Varanasi alluvium and newer alluvium consisting of fan alluvium, terrace alluvium, and recent alluvium. The geological map of the study area is shown in Fig. 1. Based on the drilling at different locations, the GSI has reported that in some part of the IGB the Quaternary alluvium lies unconformably over the basement comprising Bundelkhand Granites and sedimentary rocks of the Vindhyan supergroup. Additionally, the depth of the bedrock varies from 298 to 445 m respectively in the southern and western parts, however, in the north-eastern part the depth of the bedrock is not encountered up to the depth of 637 m.

The Himalayan along with the Ganga Plain foreland basin experiences strong compressional stress conditions; hence in the Ganga Plain, some tectonically-controlled geomorphic features are formed, or older tectonic features are reactivated to become active lineaments (Singh, 1996). Various researchers (e.g., Sastri et al., 1971; Lyon-Caen and Molnar, 1985; Burbank, 1992; Singh, 1996, etc.) have studied the tectonic framework of the Indo-Gangetic Basin. Based on the skewness of fan surface, a sudden change in the direction of alignment of the river, displacement of Siwalik hills, etc., researchers (e.g., Kumar et al., 1996; Pati et al., 2015, etc.) have reported the high neotectonic activity in the IGB.

Geophysical information shows that basement rock of the Ganga basin exhibits distinctive features. There are also few basement faults, namely Moradabad fault, Bareilly fault, Lucknow fault, Patna fault, and Malda fault (Sastri et al., 1971; Rao, 1973). The southern part of the IGB shows E-W and ENE-WSW trending linear magnetic anomaly zones (Singh, 1996). Faults within sedimentary basins are commonly associated with subtle linear anomalies in high-resolution total magnetic intensity data. The anomalies may arise from contrasts caused by tectonic juxtaposition of sedimentary layers with differing magnetic properties or from secondary magnetisation produced by geochemical activity along the fault zone (Gunn, 1997). Based on the tectonic settings, Singh (1996) has divided the IGB into three domains viz. the Piedmont Plain, the Central Alluvial Plain, and the Marginal Alluvial Plain. The Piedmont plain involves the E-W oriented Himalayan Frontal Fault, central alluvial plain dominant NW-SE trending along with WNW-ESE trending newly formed and marginal alluvial plain has SW-NE trending lineament in the basement rocks. Apart from faults, the IGB is also surrounded by important basement highs that are the Delhi-Hardwar ridge in the west, the Faridabad ridge in the middle, the Monghyr-Ghazipur ridge in the east, a poorly developed high in the Mirzapur-Ghazipur area and smaller “highs” of Raxaul, Bahraich, and Puranpur (Fig. 1).

Additionally, the IGB is one of the most seismically active regions in the world. The NW-SE trending Himalayan Frontal Fault (HFF) separates the Gangetic plain from the Siwalik hill. Any large magnitude earthquake in the Himalayan region results in huge economic and human loss. Past earthquakes in the Himalayan region like 1905, Kangra earthquake (7.8 M_w); 1934 Bihar-Nepal earthquake (8.0 M_w); 1950 Assam earthquake (8.7 M_w); 1991 Uttarkashi Earthquake (6.8 M_w) resulted in large human and infrastructure losses in the IGB. Hough and Bilham (2008) reported that Modified Mercalli intensities (MMI) during three large Himalayan earthquakes were 1–2 units higher in the basin and up to 3 units near the rivers and the floodplains. The increase of intensity in a foreland basin is a result of seismic wave amplification in the soft soils and the V_S plays an important role in its assessment. So, in this study, the V_S has been estimated for shallow and deeper depths based on the site-specific measurement and has been used to characterize seismically active region.

3. Field experiments - MASW survey in the IGB

The V_S profiles at 276 deep soil sites in the IGB were measured using the MASW active and passive (ambient noise) surveys. Active MASW and Passive (ambient noise) methods are widely used to estimate the V_S of the near-surface materials (e.g., Park et al., 1998, 2007; Park and Miller, 2008; Foti et al., 2009, 2011). The MASW emphasized the minimization of near-field and far-offset effects, sampling redundancy, acquisition speed, and overall data accuracy (Park et al., 1998). The MASW uses the inversion of dispersion curve of surface wave to estimate the variation of the V_S in a layered medium (Park et al., 1998; Xia et al., 1999; Foti et al., 2011; Lin et al., 2017; Ismail et al., 2014). Xia et al. (1999) concluded that the V_S has a great effect on the dispersion of the Rayleigh wave of the subsurface layered geological materials. However, the V_S determined from the dispersion curve of the surface wave is mainly dependent on scattered and non-source-generated surface waves, source-generated noises (i.e., body wave), and higher-mode surface wave (Park et al., 1998). Additionally, interference of noises in dispersion curve depends on frequency of waveforms and distance from the source, which can be separated according to the coherency in arrival time and amplitude in the MASW (Park et al., 1998 and Xia et al., 1999).

The MASW uses the three-step standard procedure in surface wave estimation, i.e. (1) acquiring the raw experimental data; (2) processing the signal/data to obtain experimental dispersion curve, and (3) solve the inverse problem to estimate the modal parameters. Recording of the surface waves can be done using active and passive source. When the artificial energy source (i.e., sledgehammer) is utilized in surface wave recording, it is called as active MASW survey, whereas, when it is recorded based on ambient noise (i.e., traffic or tidal waves), it is called as passive MASW (ambient noise) survey. The investigation depth is usually shallower than 50 m with the active method, whereas it can reach a few hundred meters with the passive (ambient noise) method. Most of the applications (e.g., site amplification for important structures) require V_S for deeper depths which can be either obtained from broadband sensors or heavy energy source in case of active MASW. Such sources are not only expensive but also inconvenient in field operation. To solve that, many investigators are using surface waves of natural (e.g., tidal, atmospheric etc.) and cultural (e.g., traffic) origins having low frequencies up to 1 Hz (Okada, 2003). However, to get the dispersion at lower frequencies, the passive MASW method requires 2D receiver array, which is difficult in the densely populated area. To overcome this problem, Park and Miller (2008) proposed a passive MASW technique along the roadside, which is used in this study to get the shear wave velocity profile at deeper depths. Active and passive data recorded at the same site provide different parts of the dispersion curve at different frequency bands. For investigating the V_S, Park et al. (2007) used the active and passive MASW respectively for frequency <30 and >30. Merging both the dispersion curve enhances the overall nature in extended frequencies and phase velocity ranges, results in more effective V_S profile of a site (Park et al., 2007; Foti et al., 2009).

3.1. Data acquisition and analysis

Two hundred and seventy-six MASW surveys have been carried out in the entire stretch of the IGB by dividing it into three parts i.e. PHR, UPR, and BR, which are shown in Fig. 2. Out of 276; 76, 140 and 60 MASW surveys have been done respectively in PHR, UPR, and BR. At each location, both active and passive or combined MASW survey has been done to acquire the data at shallow as well as deeper depths.

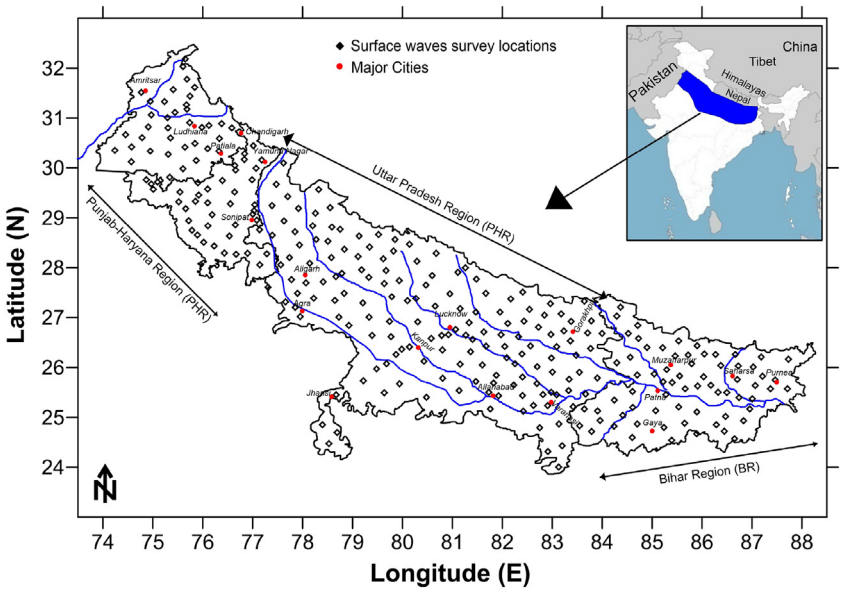

Fig. 2. MASW survey location of Indo Gangetic Basin. Separation of the IGB in to three regions is also marked.

Test setup consists of 24 channel Geode seismograph in combination with 24 vertical geophones of 2.0 Hz frequency (Fig. 3). For active survey, an impulsive source of 10 kg sledgehammer striking against a 30-cm x 30-cm size steel plate generates surface waves (Fig. 3). For active survey, the spacings between the geophones were varied from 1 to 3 m depending on the survey location. Further the distance of the source point was varied from 3 to 10 m at each location. The profile length varies from 30 m to 100 m. At each survey location minimum of 5 multiple shots were stacked to increase the signal to noise ratio (SNR). Based on field logistics, passive MASW is divided into two different types, i.e. passive remote and passive roadside MASW surveys. For acquiring the data using for passive MASW survey in the IGB, both passive remote and roadside survey have been done depending upon the availability of the space (Fig. 3). For obtaining the passive data, a passive roadside acquisition method is used by taking advantage of moving traffic which produces low-frequency ambient noise. Due to lack of proper space and number of receivers, only at 10 locations passive remote survey could be done. Circular array with diameter 50 m and triangular array with length 50 m were used for recording data using passive (ambient noise) remote survey. For obtaining the raw data using passive survey/ambient noise, different sampling intervals (2 ms to 8 ms) and recording times (30 s to 120 s) are used and to enhance the dispersion curve quality. The array length for passive survey/ambient noise varies from 60 m to 120 m. At each location multiple readings were taken to enhance the quality of raw data. After acquiring the data using both the active and passive MASW surveys, the individual dispersion curves have been extracted from velocity– frequency image. Table 1 gives the detail about the data acquisition.

The recorded raw data has been further processed to obtain the dispersion curve and finally to develop the 1D shear wave velocity profile.

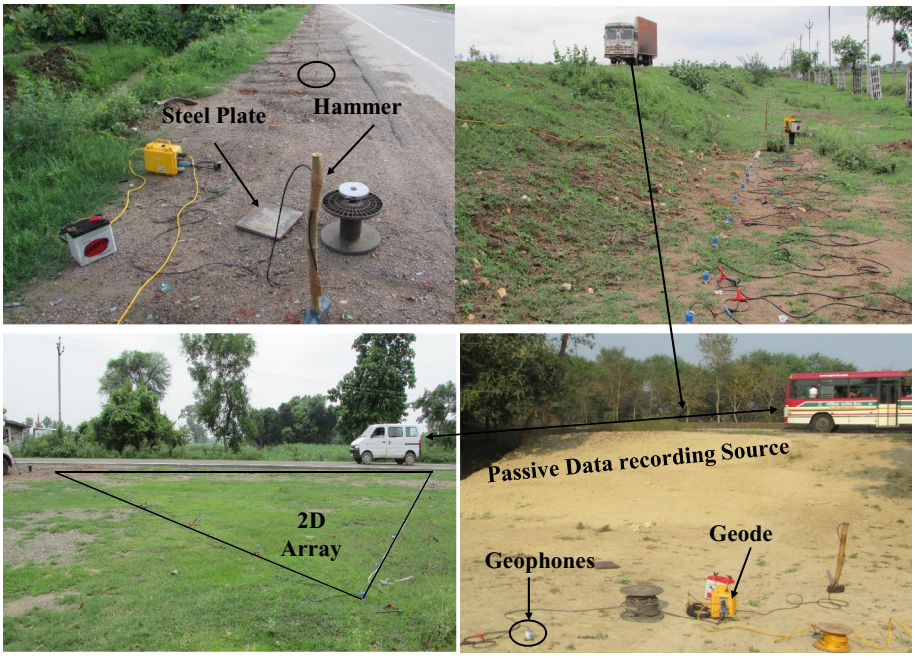

Fig. 3. Multichannel Analysis of Surface Wave instrumentation indicating the source used for active and passive survey.

Table 1
Data acquisition of MASW survey.

S. No.	Type of Survey	Number of Geophones	Spacing	Number of stacks	Recoding length	Distance from source to first receiver	Recording time
1	Active	12–24	1 to 3 m	5 to 10	1 ms	3 to 10	–
2	Passive Roadside	12–24	1 to 5 m	–	2 to 8 ms	–	10 to 120 s
3	Passive Remote	24	6 m	–	8 ms	–	60 to 120 s

The V_s profiles of each location were obtained using window-based program named 'SurfSeis 5' and 'ParkSEIS 2'. Both the software process the Rayleigh wave and generate the V_s profiles by analyzing the fundamental mode of dispersion curve of the Rayleigh wave. The dispersion curve for passive as well as active is given as Fig. 4 (a) and 4 (b) respectively. To obtain the 1D shear wave velocity curve, the obtained dispersion curve (DC) is inverted using the optimization technique defined in Xia et al. (1999). The quality of data was distinguished based on high SNR of the fundamental-mode dispersion energy. In most of the active surveys, the DC was extracted for about 5 to 70 Hz. DC having maximum SNR shows the best fit. As source to first receiver distance varied from 3 to 10 m, 8 to 10 m distance was found optimum to determine the depth of 50 m with SNR above 80% in case of active survey. For passive data, number of surveys have been done at the same location by varying the sample interval and time of recording. Each of the passive recoding was firstly evaluated independently and then superimposed on each other, afterwards smoothened to obtain the DC. DC obtained in the passive survey/ambient noise was having frequency range between 2 and 30 Hz (Fig. 4). As discussed above, for most of the data to get the enhanced shear wave velocity at lower frequency, as well as deeper depth, combined DC has been used. The dispersion curve for combined data is given as Fig. 4 (c). For getting the combined DC, the active and passive dispersion overtone image were superimposed on each other. The detailed description about combing active and passive data is given in Park et al. (2005). For majority of the cases, SNR is more that 80% in the combined active and passive curve. More explanation regarding data acquisition and processing is given in Bajaj and Anbazhagan (2019). 15 to 18 layers earth model (Park et al., 1998) is considered at initial stage of inversion. This earth model is used for determining the theoretical DC which comprises of P and S wave velocities, density value and layer thickness. Using the optimization technique (Xia et al., 1999), 1D shear wave velocity was calculated for each iteration. Several iterations were performed to get the minimum smoothening between theoretical and observed DC. Root mean square (RMS) is the best indicator for the closeness between the theoretical and observed DC. Several iterations have been performed, while the first 10 iterations showed minimum smoothing between theoretical and observed DC with the RMS error of 1% and a mean velocity variation of 5 m/s. Each DC was individually inverted to get 1D shear wave velocity profile. The match having lower RMS

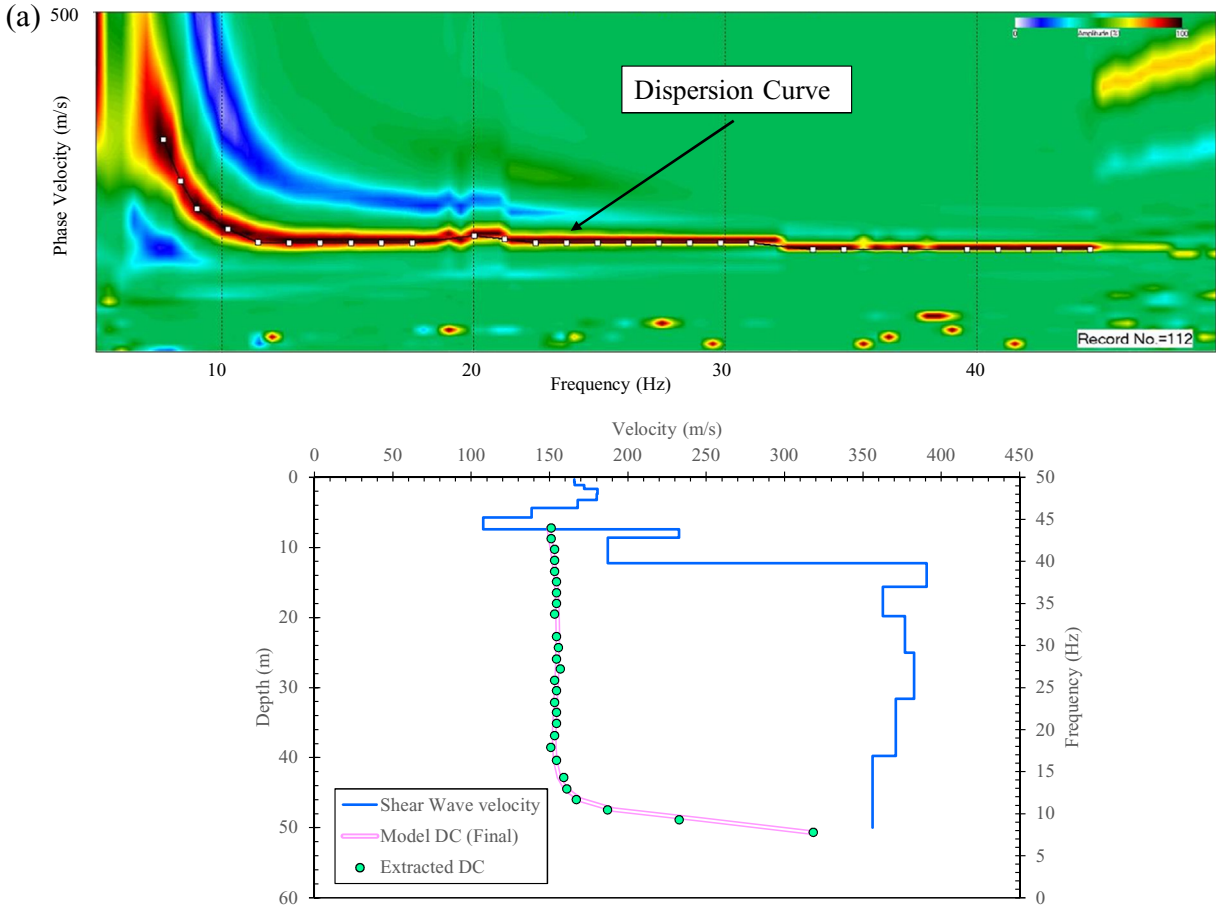

Fig. 4. Typical example showing dispersion curve and shear wave velocity for (a) active, (b) passive and (c) combined survey.

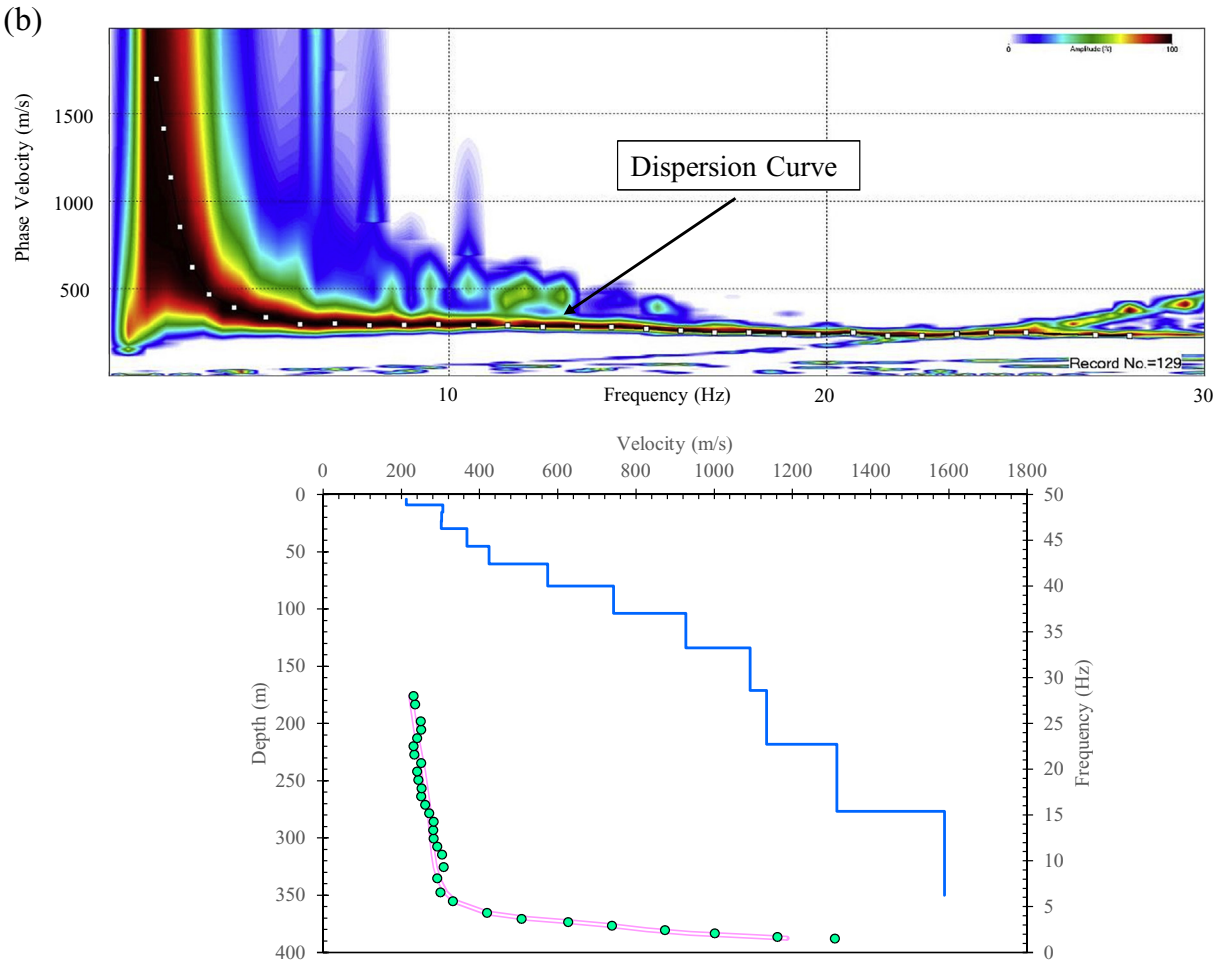

Fig. 4 (*continued*).

error value (1 to 7%) between the two curves was chosen as the final 1D shear wave velocity profile of the site.

4. Comparison of V_s with SPT-N value and lithology

The SPT is a widely used in-situ test in a borehole to evaluate the geotechnical properties of soil. The SPT-N value is widely used for geotechnical site investigation even though this method has two key problems, i.e., variable energy efficiency and overuse (Mayne et al., 2009). Hence, V_s values predicted using SPT-N value need to be used very carefully. Karabulut (2018b) explained that SPT-N value of large gravel particles should not be considered, and both the gravels and the sand need to be classified as clayey, silty, uniform and fine-grained. However, in this study, large size gravels are not observed in any of the borelog and lithological log till the considered depth. So the V_s and SPT-N value comparison and relationship has been developed irrespective of soil type or by considering all the soil type. The preliminary study has been done to compare the SPT-N value with the derived shear wave velocity for sites in PHR, UPR, and BR. As the SPT is cost-effective only to the shallow depth, so most of the SPT-N (blow count) is available maximum up to 50 m depth. All the V_s profiles that are within 50 m of in-situ SPT test have been compared. Typical example for comparison of V_s and N-Value for the three regions is given as Fig. 5. Recorded shear wave velocity profiles follow almost the same trend as compared to the SPT N value.

As mentioned above, the SPT-N value data is available up to the shallow depth. However, lithological logs (lithologs) are available for deeper depths (300 to 500 m). To check the variability of the V_s with the deposition of different layers, the V_s is also compared with the available lithologs for all the three regions and shown in Fig. 6. Lithologs within 50–100 m are also compared with the V_s profiles. The lithologs used in comparison is taken from published report under Geological Society of India (https://www.gsi.gov.in/, last accessed March 2018). It can be seen from Fig. 6 that layering the V_s profile is matching well with the lithologs. As the V_s is changing with the change in the property of the lithological layer. The V_s profiles obtained in this study show the three-distinct regions (1) a high gradient, low-velocity near-surface region, (2) an intermediate region with shear wave velocities of about 400–450 m/s, and (3) a high-velocity region at depth with velocities increasing to 600–800 m/s (Figs. 5 and 6).

5. V_S and SPT-n correlation

The correlation between the dynamic property of soil, V_s and SPT-N value is widely used in the field of earthquake geotechnical engineering. Various authors (e.g., Seed et al., 1981; Anbazhagan and Sitharam, 2008; Maheshwari et al., 2010; Anbazhagan et al., 2013, Naik et al., 2014, Rahman et al., 2016, Anbazhagan et al., 2016) have developed relationship between V_s and SPT-N value. The developed correlations are either soil dependent or region-dependent. However, limited attempts have been made to derive such relationship for the IGB. The first aim of this paper is to develop the correlation between the V_s and SPT-N. The functional form used for deriving the regression relationship between V_s and

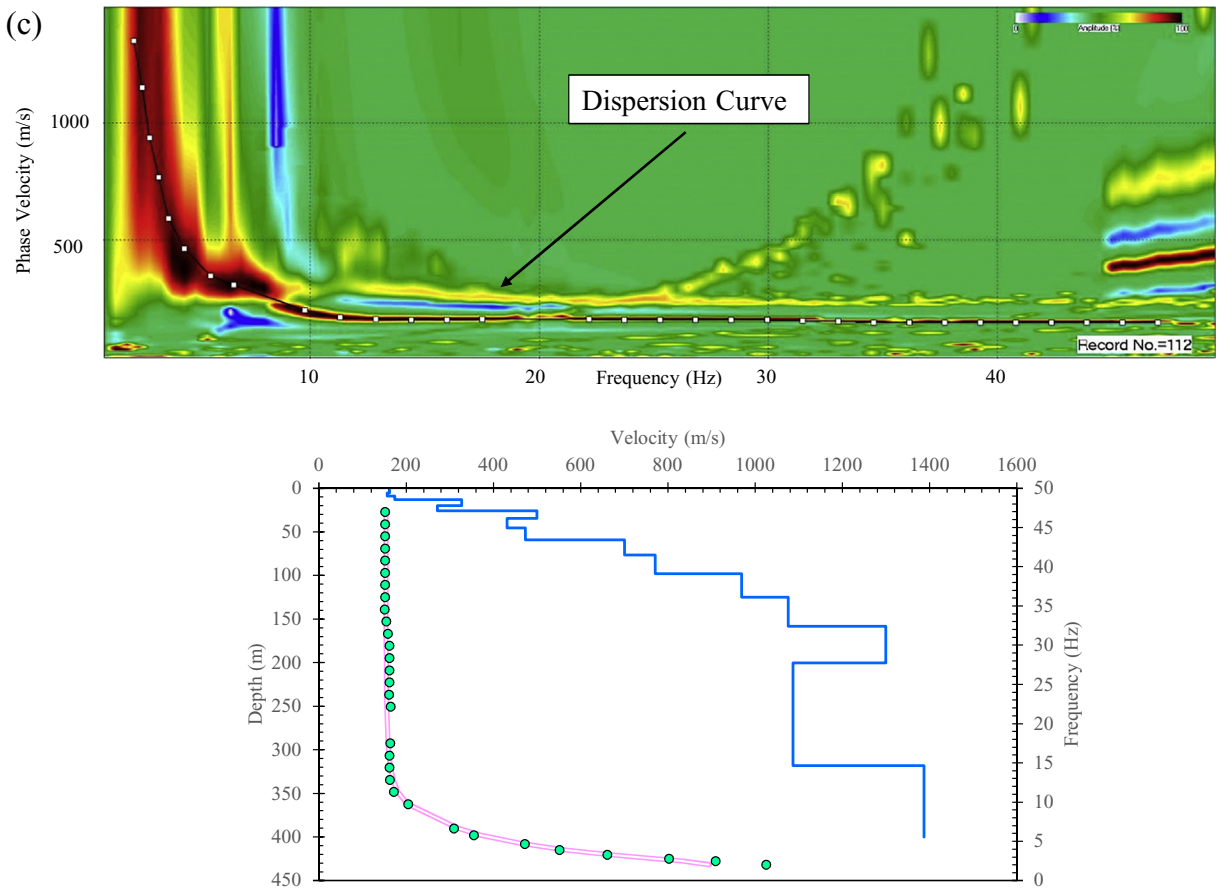

Fig. 4 (*continued*).

SPT-N value is

$$V_s = a(N)^b \quad (1)$$

where a and b are the regression coefficients and are inversely proportional to each other (Ohta and Goto, 1978; Jafari et al., 1997). Various factors such as the drilling methods, type of drill rods used, borehole sizes, sampler used, adopted blow count rate, hammer configuration, energy corrections, fines content, and testing procedures affect the SPT-N value. The combined effect of all these factors can be accounted for by applying correction factors separately or together (Anbazhagan and Sitharam 2008). In this study, both corrected and uncorrected SPT-N values are used to determine the relationship between V_s and SPT-N values. However, limited attempts have been made to evaluate these corrections for Indian soil condition and drilling practice (Anbazhagan et al., 2012). Considering Anbazhagan et al. (2012), hammer energy correction has been applied to SPT-N value for calculating the corrected SPT-N value. For PHR, UPR and BR, boreholes near to the MASW profiles were used for developing a new correlation between the V_s and SPT-N. Fig. 7 (a), (b), (c) and (d) show the correlation between the V_s and SPT-N value for PHR, UPR and BR. Both least square and orthogonal regression method are used in deriving the regression coefficients using Eq. 1. The derived coefficients for liners (lin) and uncorrected SPT-Value (UN) is given as Eq. 2, whereas for linear and corrected SPT-N (CR) value is given as Eq. 3

$$V_{sPHR\_lin\_UN} = 64.23(N)^{0.48} \pm 0.116 \quad (2a)$$

$$V_{sUPR\_lin\_UN} = 31.47(N)^{0.71} \pm 0.094 \quad (2b)$$

$$V_{sBR\_lin\_UN} = 39.41(N)^{0.58} \pm 0.127 \quad (2c)$$

$$V_{sALL\_lin\_UN} = 46.36(N)^{0.58} \pm 0.124 \quad (2d)$$

$$V_{sPHR\_lin\_CR} = 62.55(N)^{0.54} \pm 0.082 \quad (3a)$$

$$V_{sUPR\_lin\_CR} = 30.28(N)^{0.78} \pm 0.058 \quad (3b)$$

$$V_{sBR\_lin\_CR} = 38.18(N)^{0.65} \pm 0.057 \quad (3c)$$

$$V_{sALL\_lin\_CR} = 44.87(N)^{0.65} \pm 0.085 \quad (3d)$$

Further, the derived coefficients corresponding to orthogonal (orth) and uncorrected SPT-Value (UN) is given as Eq. 4, whereas for orthogonal and corrected SPT-N (CR) value is given as Eq. 5

$$V_{sPHR\_orth\_UN} = 48.86(N)^{0.61} \pm 0.087 \quad (4a)$$

$$V_{sUPR\_orth\_UN} = 21.74(N)^{0.83} \pm 0.068 \quad (4b)$$

$$V_{sBR\_orth\_UN} = 23.33(N)^{0.75} \pm 0.094 \quad (4c)$$

$$V_{sALL\_orth\_UN} = 32.95(N)^{0.68} \pm 0.101 \quad (4d)$$

$$V_{sPHR\_orth\_UN} = 43.11(N)^{0.67} \pm 0.035 \quad (5a)$$

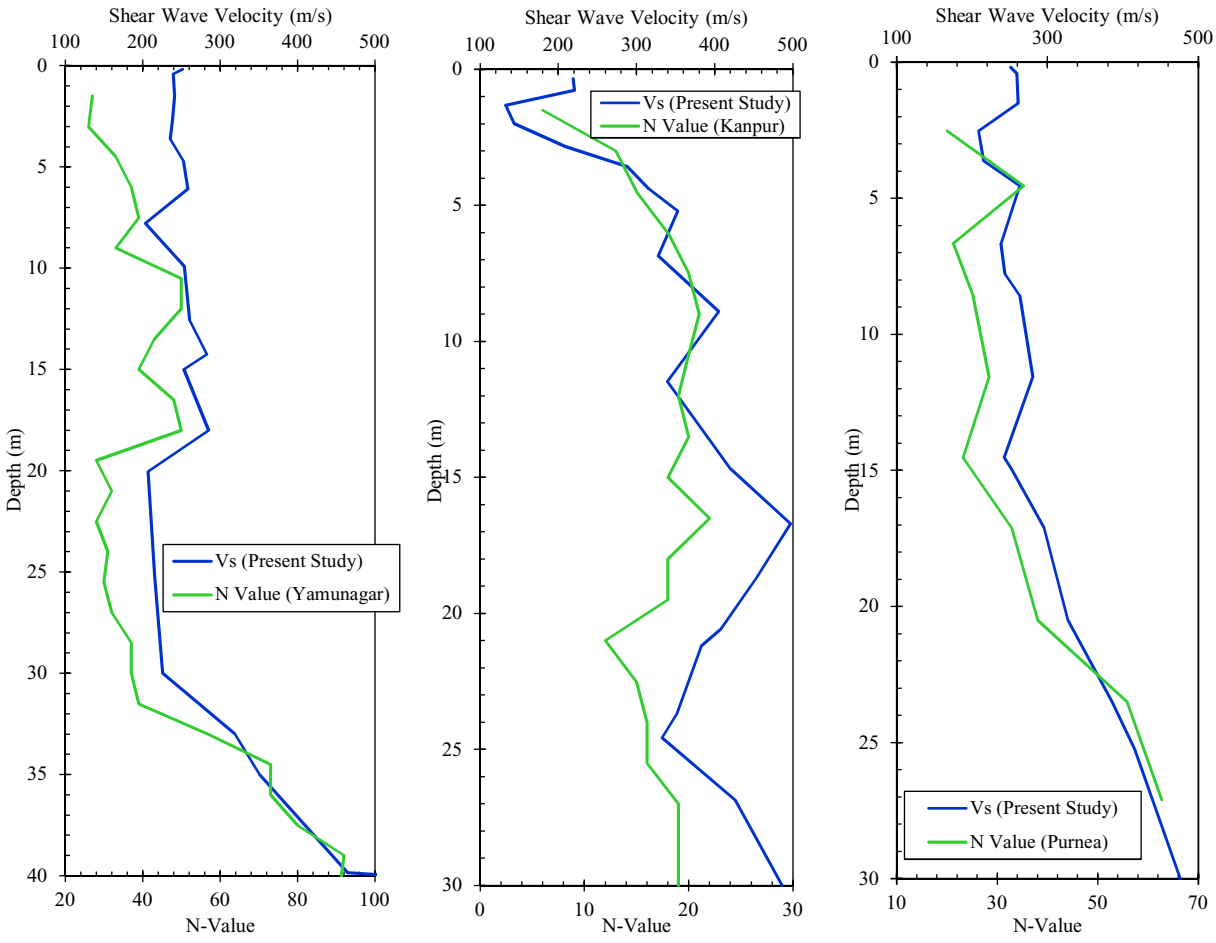

Fig. 5. Typical example for comparison of V_s and N-Value for the three regions.

$$V_{sUPR\_orth\_UN} = 20.44(N)^{0.92} \pm 0.027 \quad (5b)$$

$$V_{sBR\_orth\_UN} = 22.35(N)^{0.83} \pm 0.032 \quad (5c)$$

$$V_{sALL\_orth\_UN} = 31.77(N)^{0.76} \pm 0.044 \quad (5d)$$

The coefficients of all the equations along with standard errors are also given as Table 2. It can be noticed from Table 2 that standard error is less in case of CN. However, in many places corrected SPT-N values are not available and till date very limited documentation is available regarding energy measurement and SPT-N value corrections in India. Hence, UN SPT N and Vs relationships are also given in this study. Orthogonal regression is matching the data well at high V_s value. However, using the residual analysis, the best fit model for all the three regions has been selected.

Stafford (2014) concluded that in case of fewer data, crossed and nested mixed effect models could be employed. Hence, mixed effect model has been used for developing a relationship between V_s and N. For this purpose, data is grouped based on the region and regression equation is developed which is given as Eq. (6). Eq. 6 (a) and 6 (b) respectively represents Vs and N correlation considering uncorrected and corrected N-value. For that, *lme4* R package in Bates et al. (2013) has been used, as it provides the extremely efficient computational method for the nesting of groups for which random variables are considered. The derived equation is given as

$$\mathrm{Log}(V_s) = 1.6527 + 0.528 * \log(N) + 0.0508 * PH + 0.0613 * UP - 0.0128 * B \quad (6a)$$

$$\mathrm{Log}(V_s) = 1.6432 + 0.651 * \log(N) + 0.0407 * PH + 0.0302 * UP - 0.0098 * B \quad (6b)$$

where, PH, UP and B are dummy variables. For determining the V_s for a specific region, the value has been assigned as 1 in Eq. 6 and rest is zero. By assigning that will change the constant term of Eq. 6, which is explained with an example. For example, in case of PHR, PH is equal to 1 and rest UP and BR is equal to zero, hence Eq. (6) can be modified as $\mathrm{Log}(V_s) = 1.6527 + 0.528 * \log(N) + 0.0508 * 1 + 0.0613 * 0 - 0.0128 * 0$. The final equal for PHR is $\mathrm{Log}(V_s) = 1.7035 + 0.528 * \log(N)$. Similarly, for UPR and BR, the final Eq. 6 is $\mathrm{Log}(V_s) = 1.714 + 0.528 * \log(N)$ and $\mathrm{Log}(V_s) = 1.6399 + 0.528 * \log(N)$ respectively.

The validity of these three equations is tested based on the variation of residual with V_s. The residual value has been calculated using all the three equations. Further the variation of residual has been studied corresponding to different V_s values. The residual plot for all the equation calculated using uncorrected N-value is given as Fig. 8 (a), (b) and (c) respectively for PHR, UPR and BR. Further the residuals have been calculated for velocity bins with end points at 150, 200, 250, 300, 350, 400, 500, and 700 m/s in case of PHR and UPR (Fig. 8 (a) and (b)). Similarly, for BR, the residual has been calculated for velocity bins with end points at 200, 250, 350 and 625 m/s (Fig. 8 (c)). These residual averages at different velocity bins versus the end points of the velocity bin is also plotted in Fig. 8. The residual average corresponding to different velocity bins is used for determining the robustness of different equations derived in this study. Similar plot has been given for corrected N-value as Fig. A1 (appendix). Based on the variation of residuals, it can be concluded that the mixed effect relation (Eq. 6) is predicting better till the

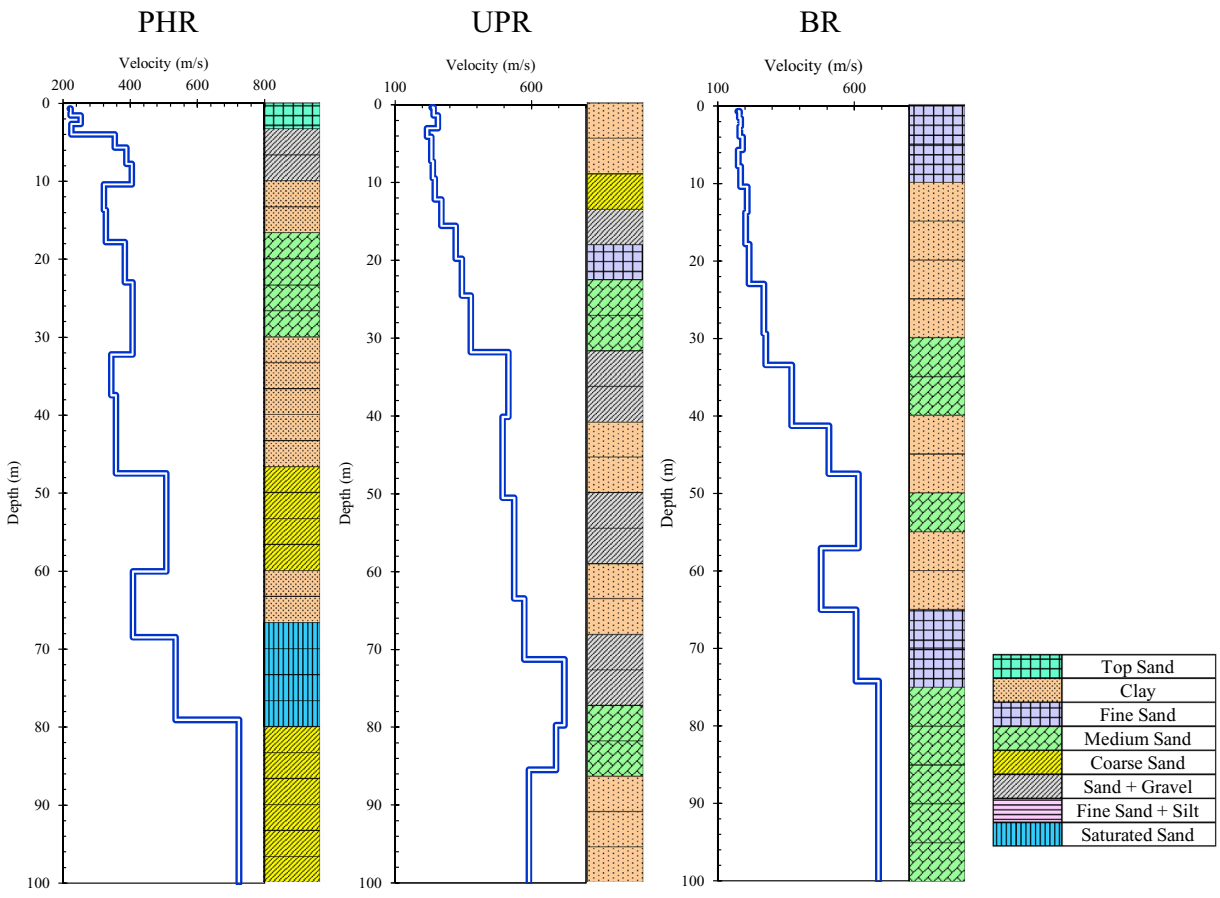

Fig. 6. Typical example for comparison of V_s and lithologs for the three regions.

$V_s \leq 250$ m/s in case of PHR and UPR (See mixed (M) in Fig. 8 and A1). Whereas, coefficient derived using least square analysis is predicting well in the case of BR (See linear (M) in Fig. 8 (c) and A1 (c)). However, in case of $V_s > 250$ m/s, coefficient derived using orthogonal analysis is predicting well in all the three cases (Fig. 8 and A1). For future work, it can be recommended that if less data is available, the V_s and SPT-N can be derived using orthogonal regression analysis instead of least square analysis. It can be noted that these correlations are rough estimation of V_S from available SPT-N value and can be further tested by estimating the V_s using direct methods in future. Hasançebi and Ulusay (2007) mentioned that SPT-N is a significant parameter in V_s and SPT-N correlation, whereas the type of soil has relatively less influence. The use of V_s and SPT-N correlation with uncorrected SPT-N value is appropriate for determination of V_s value (Hasançebi and Ulusay, 2007). Many researchers (e.g. Dikmen, 2009; Hasançebi and Ulusay, 2007) commented on the reliability of V_s and SPT-N correlation for clayey soils. The derived coefficients can be used for all types of soil.

The comparison of all the regression equations developed in this study is given as Fig. 9(a)and 10(a). Figs. 9 and 10 respectively show the comparison of V_s-SPT-N (uncorrected) and V_s-SPT-N (corrected) developed in this study using all the three models. For the same SPT-N value (i.e., SPT-$N > 25$), UPR (orth) is predicting high V_s as compared to another equation. That can be justified considering the geological deposit as most part of UPR is lying over older alluvium. A significant difference can be observed while calculating the V_s considering BR (lin), BR (orth) and BR (mixed) relationships when the SPT N-value exceeds 30. However, based on the residual analysis it has been seen that BR (orth) is predicting well for all set of SPT-N values.

Many researchers developed a relationship between the V_s and SPT-N in different parts of the world (Fujiwara, 1972; Imai and Tonouchi, 1982; Jafari et al., 1997; Pitilakis et al., 1999; Akin et al., 2011; Anbazhagan and Sitharam, 2008; Andrus et al., 2006; Dikmen, 2009; Hanumantharao and Ramana, 2008; Hasançebi and Ulusay, 2007; Kiku et al., 2001; Kuo et al., 2012; Anbazhagan et al., 2016 etc.). However, in this study V_s and SPT-N developed for the Indian subcontinent is compared with the newly developed relationships. Fig. 9(b) and (c) show the comparison of currently developed V_s and SPT-N (uncorrected) relation with the existing one within Indian subcontinent. Similarly, Fig. 10(b) and (c) show the comparison of currently developed V_s and SPT-N (corrected) relation with the existing one within the Indian subcontinent. Fig. 9(b) and (c) and Fig. 10(b) and (c) show the comparison considering the V_s and SPT-N (corrected and uncorrected) relation developed using least square and orthogonal approach. Hanumantharao and Ramana (2008), Maheshwari et al. (2010) and Anbazhagan et al. (2013) developed the V_s and SPT-N relation considering uncorrected SPT-N value respectively for Delhi, Chennai and Lucknow regions. Anbazhagan and Sitharam (2008) and Naik et al. (2014) used the corrected SPT-N value for developing the V_s and SPT-N value relationship respectively for Bangalore and Kanpur regions. Kanpur and Lucknow cities in UPR lies in the current study area. UPR (lin) is matching well with Anbazhagan et al. (2013) for the SPT N-value >40 and with Naik et al. (2014) for SPT-N <30. The reason may be considering the wide area while developing current correlation between the V_s and SPT-N value.

6. Spatial variation of V_S and seismic site classification of the IGB

Hazard level at the surface is generally estimated using ground motion at bedrock and the dynamic properties of the soil profile. Commonly, site response analysis is used in calculating the site amplification and which is further used in estimating the ground motion at surface. Average shear wave velocity at the top 30 m depth (V_{s30}) is an important parameter for

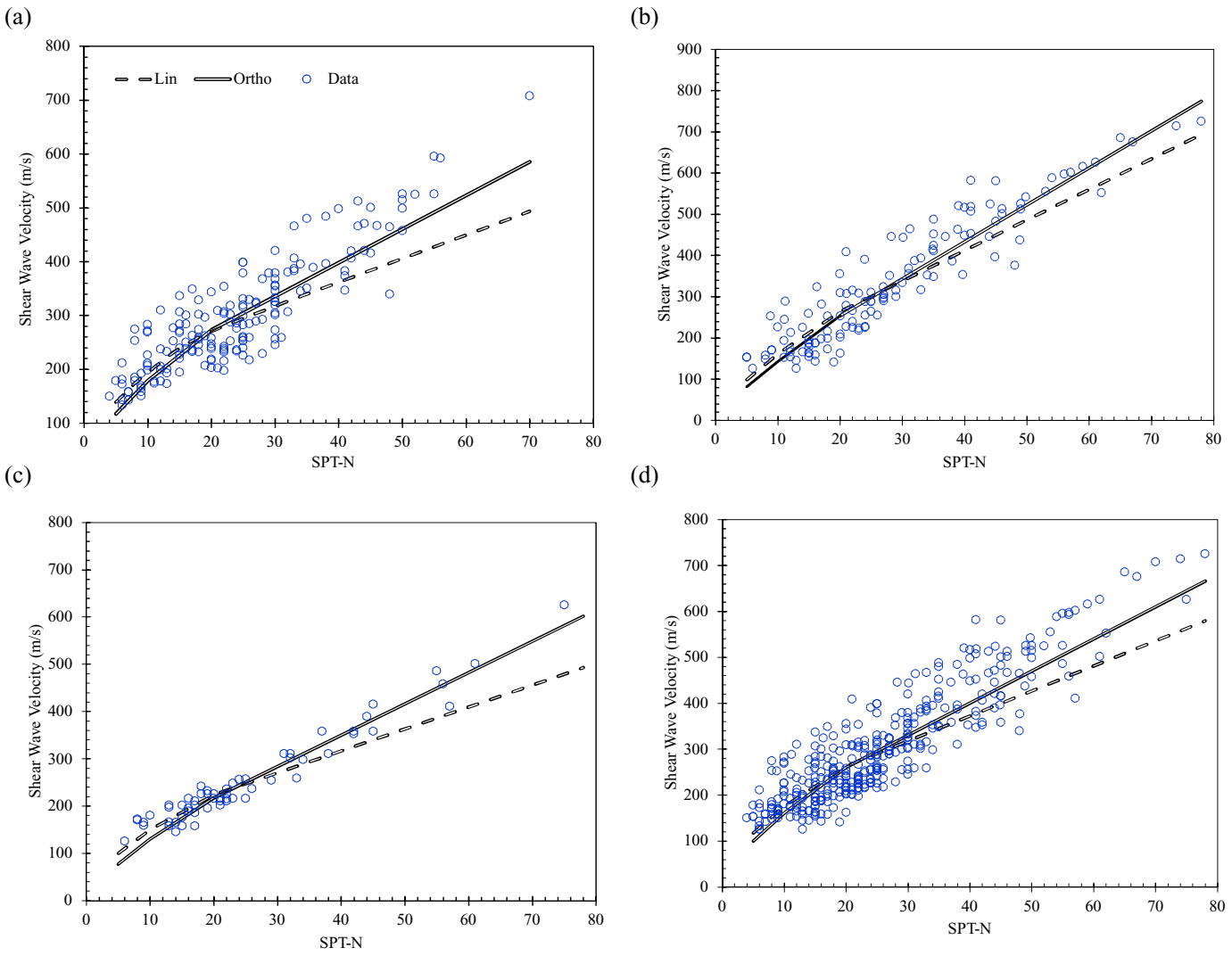

Fig. 7. V_s and SPT-N correlation for (a) PHR, (b) UPR, (c) BR and (d) All data using linear least square (lin) and orthogonal (ortho) regression approach.

site characterization in estimating the site amplification. It is calculated as

$$V_{s30} = \frac{\sum_1^N d_i}{\sum_1^N \frac{d_i}{V_{si}}} \tag{7}$$

Table 2
Derived regression coefficients between V_s and SPT-N using $V_s = a(N)^{b.}$

S. No.	Region	N-Value description	Regression Type	a	b	σ
1	PHR	UN	Least Square (lin)	64.23	0.48	0.116
			Orthogonal (orth)	43.86	0.61	0.087
		CN	Least Square (lin)	62.55	0.54	0.082
			Orthogonal (orth)	43.11	0.67	0.035
2	UPR	UN	Least Square	31.47	0.71	0.094
			Orthogonal	21.74	0.83	0.068
		CN	Least Square	30.28	0.78	0.058
			Orthogonal	20.44	0.92	0.027
3	BR	UN	Least Square	39.41	0.58	0.127
			Orthogonal	23.33	0.75	0.094
		CN	Least Square	38.18	0.65	0.057
			Orthogonal	22.35	0.83	0.032
4	All	UN	Least Square	46.36	0.58	0.124
			Orthogonal	32.95	0.68	0.101
		CN	Least Square	44.87	0.65	0.085
			Orthogonal	31.77	0.76	0.044

where, d_i is the thickness of layer i and V_{si} is the shear wave velocity of the layer i and V_{s30} is the average shear wave velocity in the top 30 m. Time average shear wave velocity up to 30 m depth has been calculated for all the three regions i.e. PHR, UPR and BR. The NEHRP, USA and Eurocode 8 (EC8) use the V_{s30} for site classification to determine the amplification factors. As for India, there is no such provision, hence, in this study the near-surface material has been classified using V_{s30}-based NEHRP and EC8 classifications (Table 3). Fig. 11(a) and (b) show the variation of V_{s30} in the IGB as per NEHRP and EC8. It can be seen from Table 3 that, site class and description is different for both the codes, however, in this study, site class described by the NEHRP is used for further discussion. As for the Indian subcontinent, NEHRP seismic site classification has been widely followed for seismic site classification instead of EC8. About 22% of the sites in BR is of site class E with the V_{s30} between 143 m/s and 176 m/s. Majority of the sites in UPR is of site class D, however in PHR, mostly site class are either C or D. Most of the sites near to the Kosi, Satluj and Gomati rivers is of seismic site class E. The V_{s30} near to Kosi region varies from 147 to 172 m/s and near to Satluj in PHR, V_{s30} varies from 160 to 175 m/s. Most of the sites in the southwest side of Yamuna in UPR is of site class B, which are due to the presence of Bundelkhand Faridabad ridge and Archean granites and Precambrian Metamorphic (Fig. 1). The V_{s30} in that region varies from 822 to 1136 m/s. Similarly, due to the presence of Munger-Saharsa Ridge and Paleozoic granite in the south of Ganga in BR, most of the sites are either site class B or C.

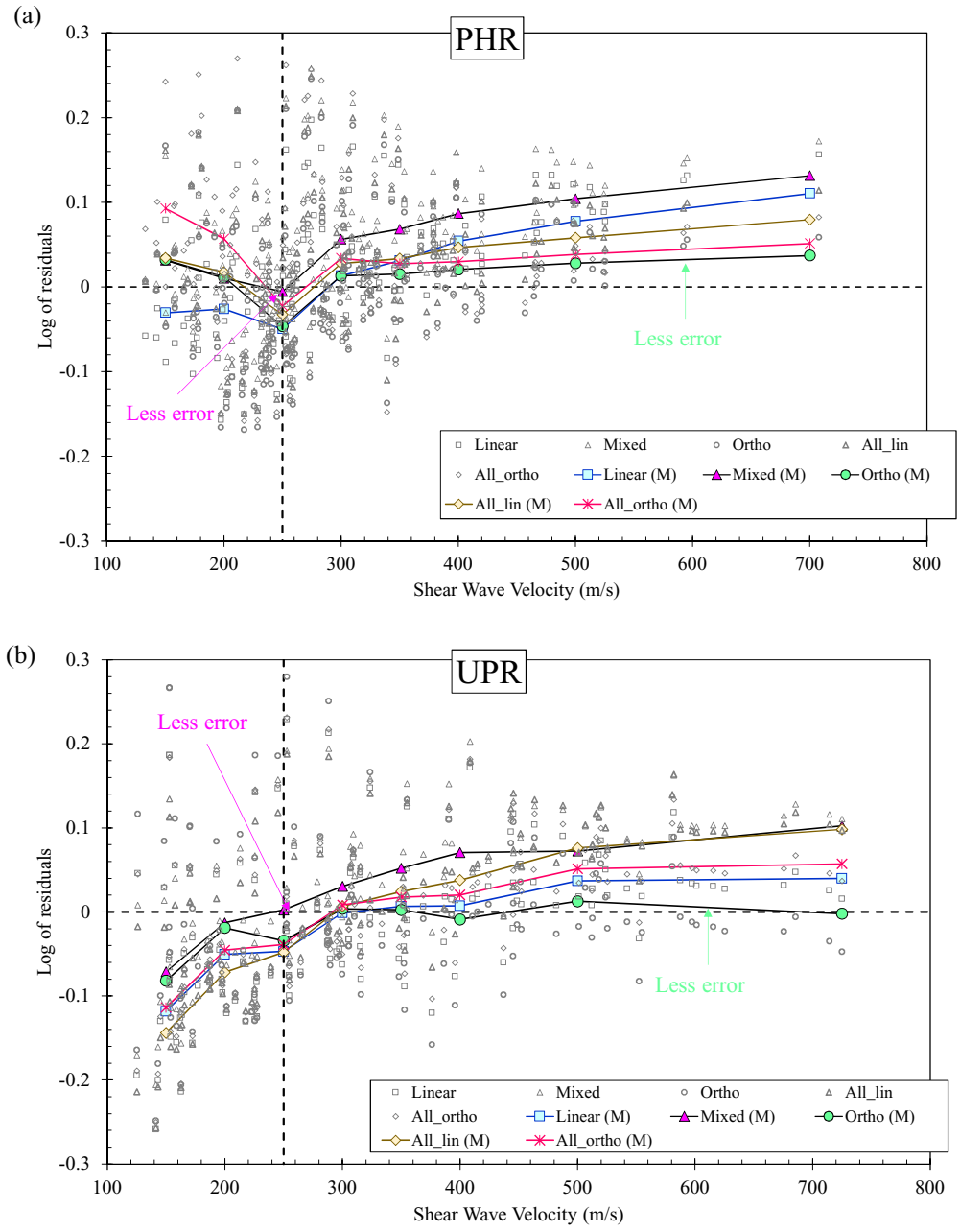

Fig. 8. Residual versus shear wave velocity curve for (a) PHR, (b) UPR and (c) BR for determining the best suitable regression model between V_s and SPT-N values.

The V_{s30} in that region varies from 450 to 1152 m/s. Many of the sites in the northeast side of UPR and BR is of site class B and C, which are due to the presence of Siwalik Hills (Figs. 1 and 10). For PHR region the V_{s30} varies from 160 to 180 m/s, 206 to 340 m/s, 382 to 620 m/s and 795 to 1251 m/s respectively for site class E, D, C and B. For UPR V_{s30} varies from 147 to 180 m/s, 247 to 358 m/s, 401 to 630 m/s and 822 to 1136 m/s respectively for site class E, D, C and B. For BR region V_{s30} varies from 143 to 176 m/s, 214 to 354 m/s, 387 to 615 m/s and 775 to 1152 m/s respectively for site class E, D, C and B. The summary of variation of V_{s30} for all the three regions is given as Table 4. Further, the contours of variation of V_{s30} have been drawn over the entire study area. For few of the locations due to inaccessibility and political reasons, the MASW survey could not be done. For those locations, the V_{s30} is predicted based on geological map (Fig. 1) and the V_{s30} map (Fig. 11). The contours of variation of the V_{s30} have been drawn and given as Fig. 12. It can be seen from Fig. 12 that in PHR and BR, most of the site class D has the V_{s30} between 180 and 270 m/s, whereas in UPR it varies from 270 to 360 m/s. Maximum value of V_{s30} is observed in southeast of Sutlej river in PHR, southwest of Yamuna river in UPR and south part of Ganga river in BR as explained above. Most of the sites on Delhi-Haridwar ridge is either site class B or C (Figs. 11 and 12).

In the PHR region, the average shear wave velocity till top 5, 10, 15, 20, 30, 50, 100, 150, 200, 250 and 300 m depth is 168–732, 156–785, 164–820, 167–985, 160–1251, 202–1328, 282–1538, 235–1853, 345–2012, 372–2247, and 402–2462 respectively. The V_s along Satluj and Beas rivers is 200 to 250 m/s for top 10 m which may be due to the presence of loose sand available near to the course of these rivers. The velocity near to the northeast part of Punjab is high at 300 m as compared to another part which may be due to the presence of granite or angular quartzite after 250 m depth (GSI, 2012). The UPR is mostly dominated by clay and

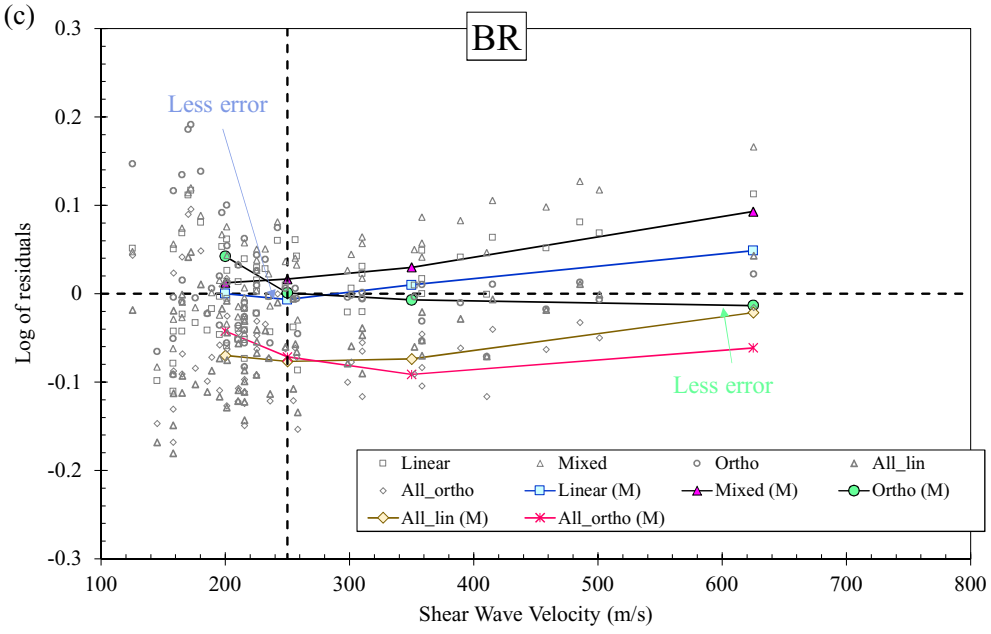

Fig. 8 (*continued*).

sand at different depths. As per the geological quadrangle available for different places, UPR is covered with alternative layer of clay and sand with kankar or gravel (https://www.gsi.gov.in/). The average shear wave velocity till top 5, 10, 15, 20, 30, 50, 100, 150, 200, 250 and 300 m depth is 162–425, 174–495, 152–632, 175–885, 147–1136, 186–1096, 280–1372, 325–1985, 434–1691, 495–1791 and 415–2800 m/s respectively. The shear wave velocity near to the upper Ganga plain is 215 ± 20 m/s till 10 m depth and increases to 750 ± 50 m/s till 150 m depth, which is

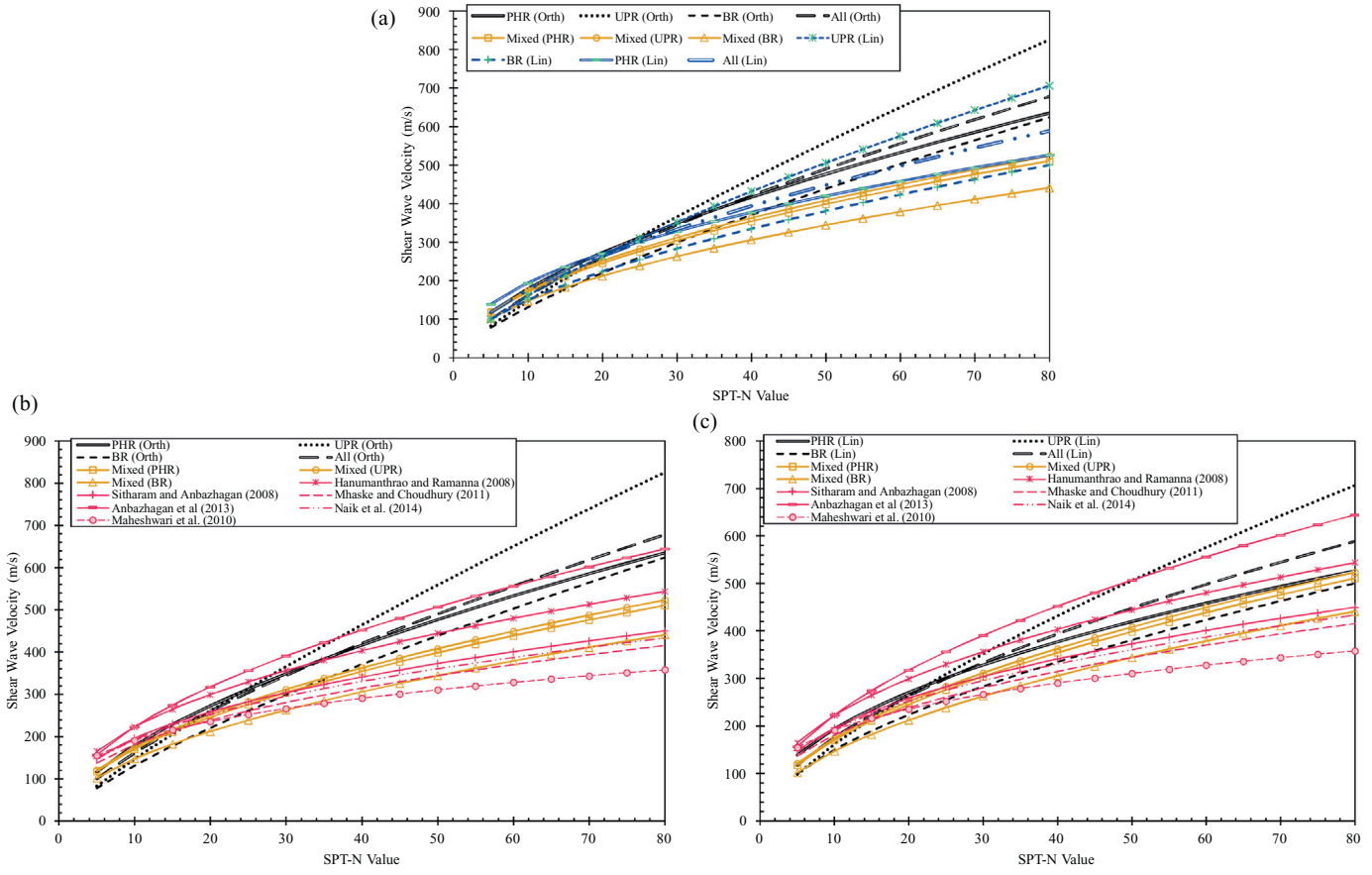

Fig. 9. Comparison of V_s and SPT-N (uncorrected) (a) developed in this study using least square, orthogonal and mixed effect models. Comparison of present study model considering (b) least square (lin) and (c) Orthogonal (orth) model with the correlation developed for Indian subcontinent.

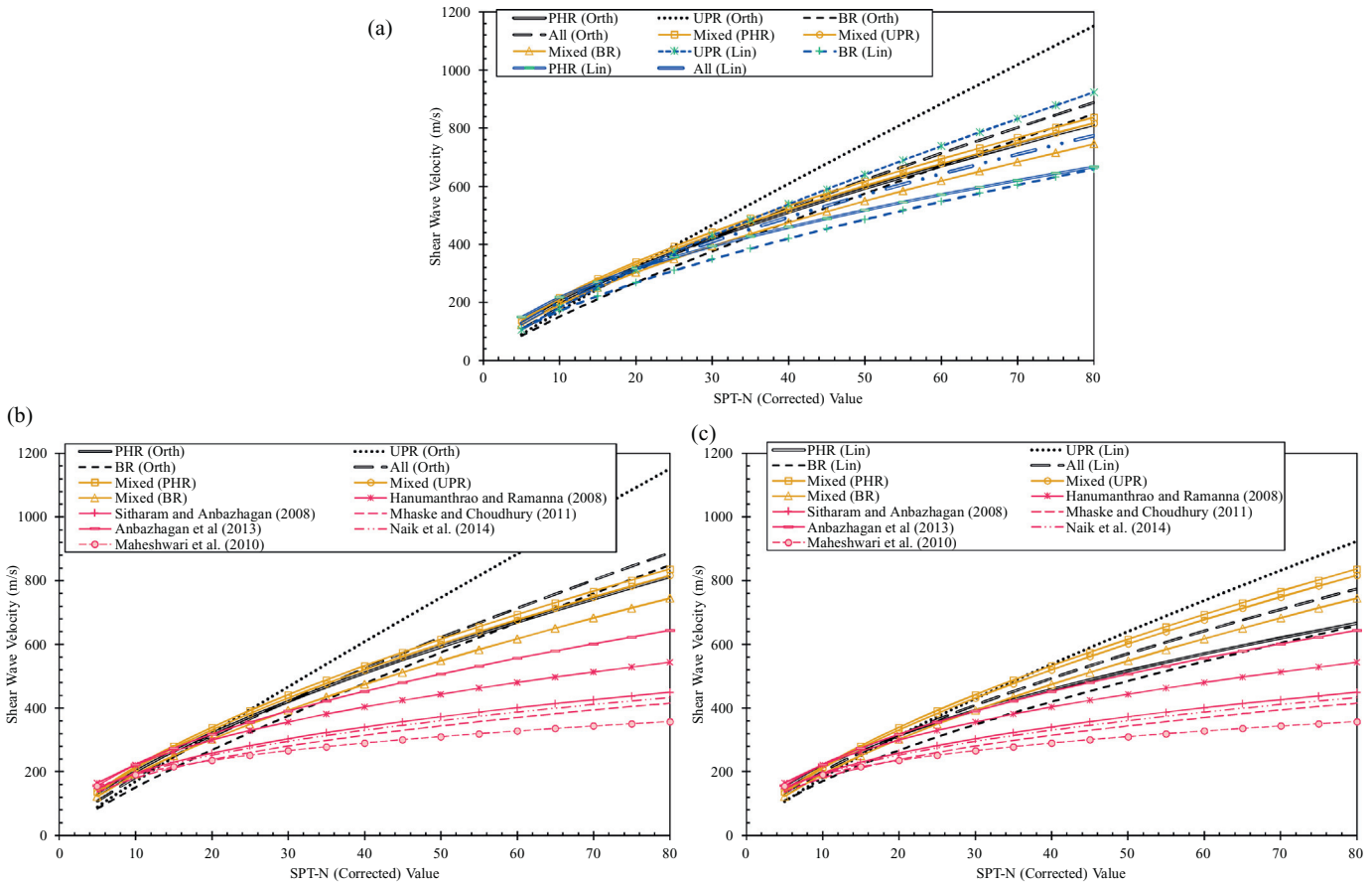

Fig. 10. Comparison of V_s and SPT-N (corrected) (a) developed in this study using least square, orthogonal and mixed effect models. Comparison of present study model considering (b) least square (lin) and (c) Orthogonal (orth) model with the correlation developed for Indian subcontinent.

Table 3
Seismic site classification as per NEPHP and Eurocode 8

NEHRP, USA			Eurocode 8		
Site Class or soil profile type	Description	Average shear wave velocity in the top 30 m	Subsoil class	Description of stratigraphic profile	Average shear wave velocity at top 30 m
A	Hard Rock	>1500	–	–	–
B	Rock	760–1500	A	Rock or other rock-like geological formation, including at most 5 m of weaker material at the surface	>800
C	Very Dense soil/soft rock	360–760	B	Deposits of very dense sand, gravel or very stiff clay, at least several tens of m in thickness, characterized by a gradual increase of mechanical properties with depth	360–800
D	Stiff soil	180–360	C	Deep deposits of dense or medium-dense sand, gravel or stiff clay with thickness from several tens to many hundreds of m	180–360
E	soft soil	<180	D	Deposits of loose to medium cohesionless soil (with or without some soft cohesive layers), or of cohesive soil predominantly soft-to-firm	<180
F	Special soil requiring site-specific evaluation (1. Soils vulnerable to potential failure or collapse under seismic loading e.g., liquefiable soils, quick and highly sensitive clays, collapsible weakly cemented soils; 2. peats and/or highly organic clays (3 m or thicker layer); 3. very highly plasticity clays (8 m or thicker layer with plasticity index>75); 4. very thick soft/medium stiff clays (36 m or thicker layer)		E	A soil profile consisting of a surface alluvium layer with Vs30 values of class C or D and thickness varying between about 5 m and 20 m, underlain by stiffer material with Vs30 > 800 m/s	–
			S1	Deposits consisting - or containing a layer at least 10 m thick of soft clays/silts with high plasticity index (PI>40) and high-water content	<100
			S2	Deposits of liquefiable soils, of sensitive clays, or any other soil profile not included in classes A-E or S1	–

due to the thick deposits of Varanasi older alluvium, as indicated by the GSI Lucknow quadrangle. The upper silt-clay is underlain by the yellow sand near to the channels in the area around the middle Ganga region (Gorakhpur quadrangle, GSI). Average V_s in this area varies from 230 ± 30 m/s to 310 ± 25 m/s upto 30 m depth. Southwestern part of UPR is occupied by reddish and whitish, fine-grained, compacted quarzitic

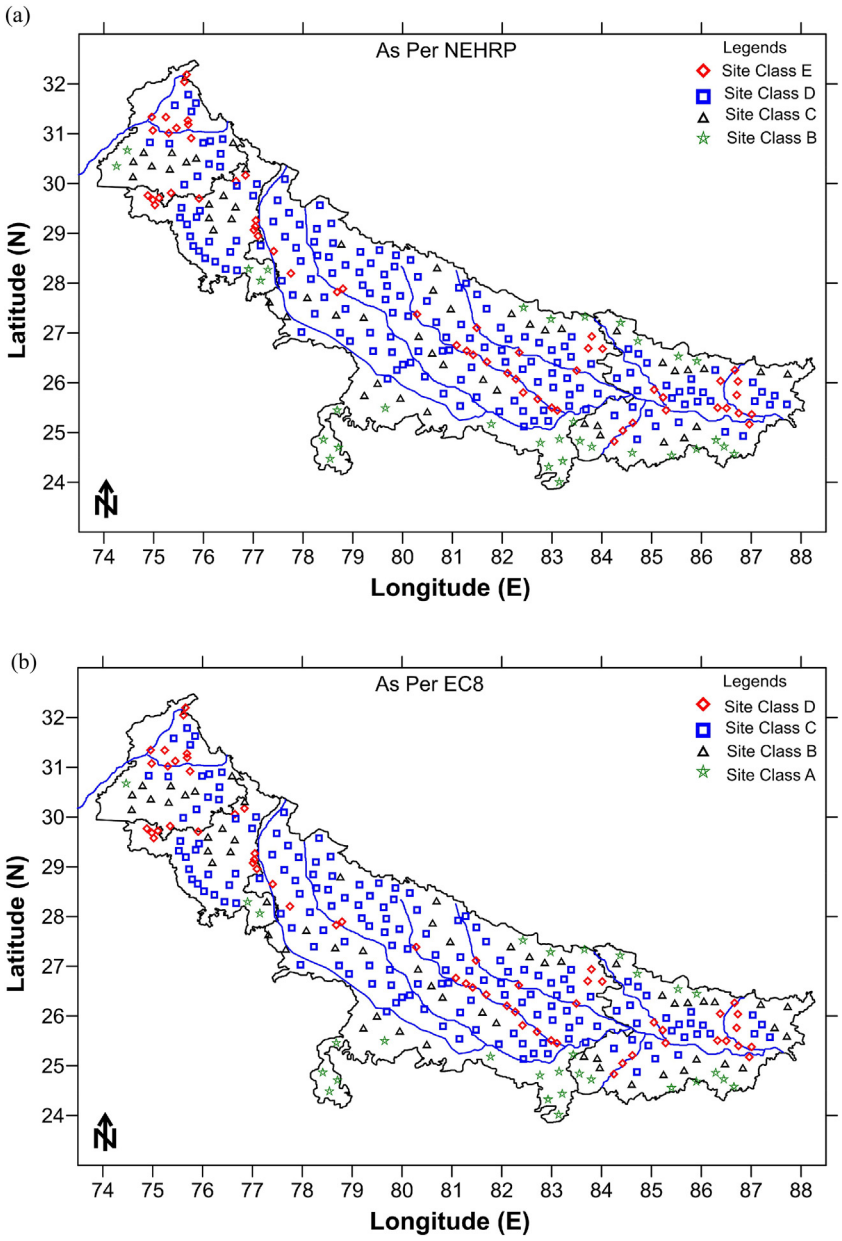

Fig. 11. Seismic site classification of MASW survey location of Indo Gangetic Basin using (a) NEHRP and (b) EC8 seismic site class.

sandstone (Varanasi quadrangle, GSI). Average V_s near to this region is more as compared to other parts of UPR even at shallower depths i.e. 450 ± 30 m/s till 10 m depth and increased to 810 ± 50 m/s till 75 m depth. The average shear wave velocity till top 5, 10, 15, 20, 30, 50, 100, 150, 200, 250 and 300 m respectively varies from 160 to 685, 155–758, 170–913, 157–1188, 143–1152, 190–1273, 219–1187, 210–1875, 372–1950, 403–2014, 445–2227 m/ s in BR. However, the V_s for different regions in BR is also compared and high spatial variability in V_s is observed.

Table 4
Summary of soil classification and summary of V_s for different regions

S. No.	Region	V_{s30} range (m/s)	Classification as per NEHRP	Range of V_{s30} (m/s)	V_{s150} range (m/s)	V_{s300} range (m/s)
1	PHR	160–1251	B	795 to 1251	1102 to 1853	2000–2462
			C	382 to 620	571 to 1025	852 to 1528
			D	206 to 340	472 to 752	552 to 1082
			E	160 to 180	235 to 436	402 to 888
2	UPR	147–1136	B	822 to 1136	1428 to 1985	1985 to 2800
			C	401 to 630	672 to 1492	846 to 2197
			D	247 to 358	428 to 854	591 to 1480
			E	147 to 180	325 to 720	415 to 750
3	BR	153–1152	B	775 to 1152	1272 to 1875	1857 to 2227
			C	387 to 615	522 to 1220	807 to 1868
			D	214 to 354	422 to 698	527 to 1025
			E	143 to 176	210 to 401	445 to 728

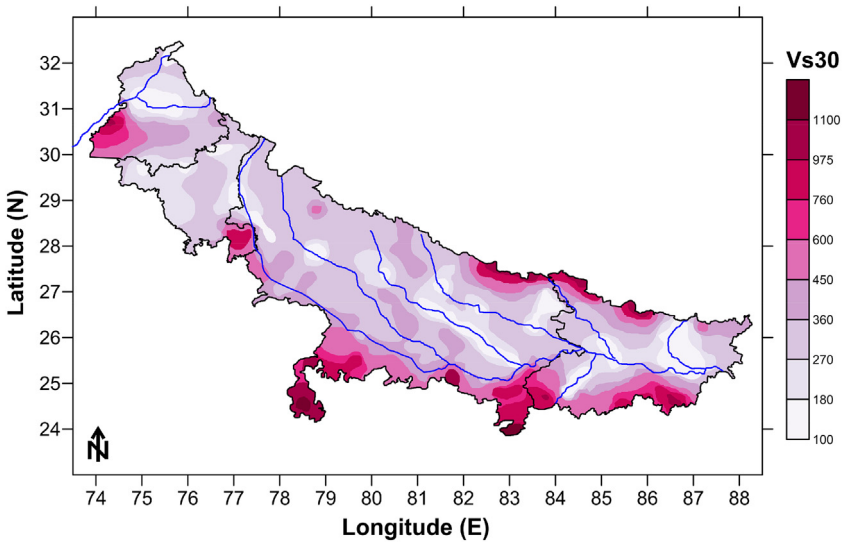

Fig. 12. Spatial variability of time average shear wave velocity at 30 m depth (V_{s30}) for Indo Gangetic Basin.

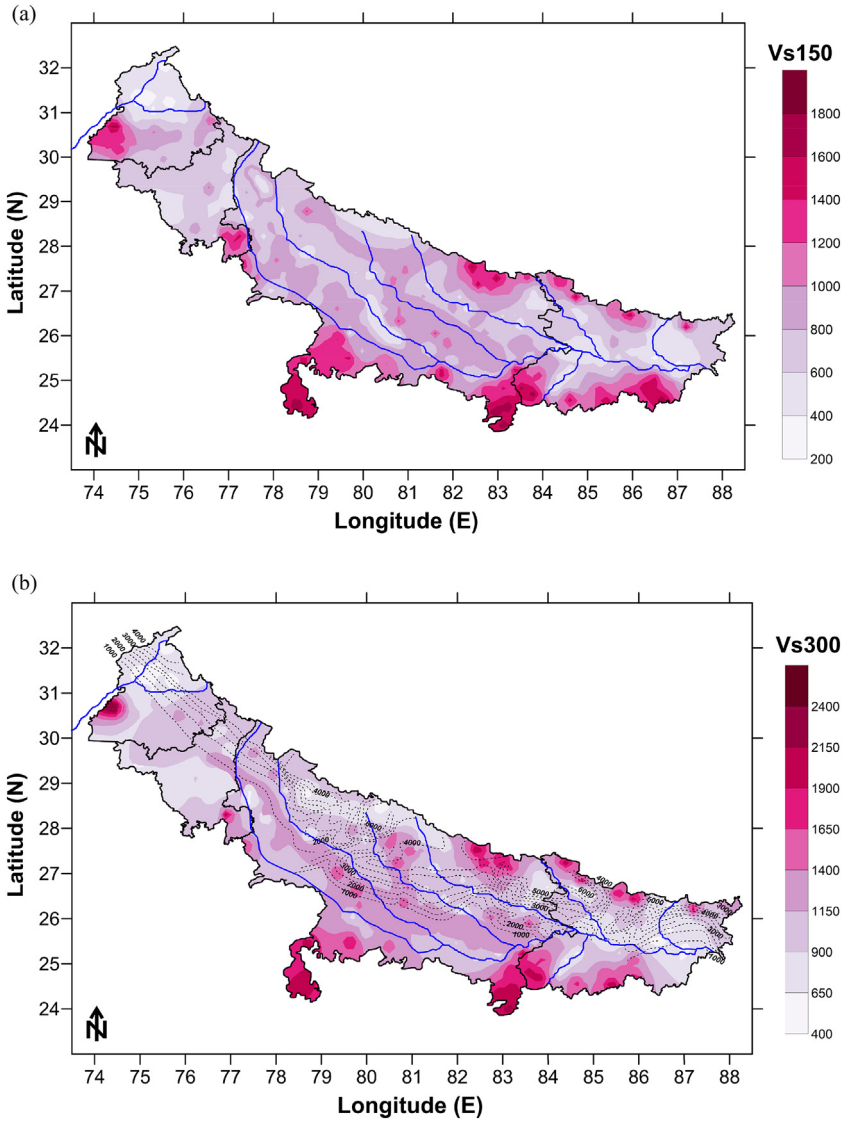

Fig. 13. Spatial variability of time average shear wave velocity at (a) 150 m depth (V_{s150}) and (b) 300 m depth (V_{s300}) for Indo Gangetic Basin.

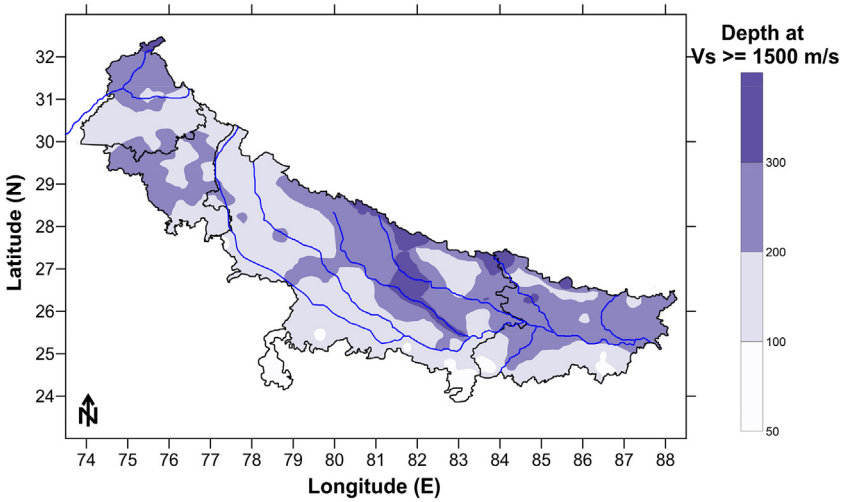

Fig. 14. Spatial variability of depth at which V_s is equal to and >1500 m/s.

The upper 50 m near to Sone megafan in BR region is occupied by clay/muddy deposits underlined by brownish yellow fine to coarse sand interleaved with gravel layers (Sahu et al., 2015). The V_s in this region is 250 ± 30 m/s up to 50 m depth, due to the presence of dark grey hard clay in the alternative alternating with grey silt and fine sand (Muzaffarpur quadrangle, GSI). The V_s in the south part of BR is high, as this part is covered with isolated ridges and mounds and hills and highlands of the Chotanagpur Plateau (Gaya quadrangle, GSI). The V_s to 30 m depth in the Kosi and Gandak basin is 170 ± 20 m/s and 210 ± 30 m/s is significantly low as compared to average shear wave velocity of PHR and UPR.

Seismic regulations of many countries use the V_{s30} for site classification. Despite of its widespread use, there is no universal agreement that the V_{s30} is a valid parameter for site amplification (Castellaro et al., 2008). Wald and Mori (2000) and Mucciarelli and Gallipoli (2006) doubted about the validity of the V_{s30} as a proxy to soil amplification in tectonically active region or geological setting. The role of deeper sediments (>30) in estimating site amplification was shown by Frankel et al. (2002) and Park and Hashash (2004). Lee and Trifunac (2010) also raised an issue about the V_{s30} as a meaningful parameter in estimating the strong ground motion and emphasize on the thickness of soil column in evaluating site amplification. Hence, in this study an attempt has been made to calculate the time average shear wave velocity by considering different depths of the soil column. Therefore, average shear wave velocity at the top *z* meter (V_{sz}) with z at 50 m, 100 m, 150 m, 200 m, 250 m, and 300 m has been calculated. Variation of V_{s150} and V_{s300} in the study area is given as Fig. 13 (a) and 13 (b). On comparing Fig. 13(a) with Fig. 12, it has been observed that, for few areas like Punjab-Haryana border or near Gomati river in UPR, where the V_{s30} is between 160 and 180 m/s, however, the V_{s150} is from 325 to 720 m/s. This refers to that even thought, loose material is available till top 30 m, but medium to dense soil extend up to depth of >150 m. Similarly, near to Ganga river in UPR, the V_{s30} is between 360 and450 m/s, however, the V_{s150} is between 430 and 600 m/s, which indicates the presence of low velocity material between 30 and 150 m depth and the dense layer is not encountered up to 150 m depth. Similar observation is seen in the confluence of Ganga, Sone and Gomati river in BR. Based on the variability of the V_{s30} and V_{s150} variation along the depth, it can be concluded that low velocity region is also present at deeper depth in the IGB, especially near to active sedimentation area. Hence, considering 30 m depth is a weak proxy for site amplification estimation, this is an indication that for deeper soil sites, the V_{s30} is not the valid parameter for site amplification. As this is not the aim of this paper, it will be studied in future work.

Based on geophysical study and deep drilling carried out by Oil and Natural Gas Corporation (ONGC), various researchers (Sastri et al., 1971; Singh, 1996) interpreted the sub-surface geology and basement thickness. According to Singh and Singh (1992), average alluvial fill in the IGB decreases from the foothill in the north to the south and thins out as a mere veneer on the Peninsular margin. As per Rao (1973), the depth of basement is at about 6000 m near to the Sivalik foothill zone and decreases gradually (see contours in Fig. 13 (b)). As in most of the profiles, the V_s is determined up to the maximum depth of 300 m, the average shear wave velocity for the top 300 m (V_{s300}) is calculated and compared with the basement depth map and given as Fig. 13(b). It can be seen from Fig. 13 (b) that the V_{s300} is in between 400 and 900 m/s near to the foothill in the north and it has increased to 2150 m/s in the south. However, some part in the foothills has high velocity which may be due to the presence of rocky terrain due to nearby the Himalayan range (i.e. HFT). However, in few parts of the IGB, where deeper depth of the basement is predicted, have high V_{s300} that may be due to the presence of older alluvium and low sedimentation in that areas (e.g. near to Gomati river). In most of the part in UPR and BR, the basement depth is correlating well with V_{s300} (Fig. 13 (b)). However, in most part of the PHR, constant V_{s300} is observed which may be due to the presence of quartzites and granites of Delhi supergroup.

Further the spatial variation of depth at which shear wave velocity is >1500 m/s is also studied. The variation of depth is given as Fig. 14. It can be noted that for the whole IGB V_s >1500 m/s is observed at different depths. This may be due to the variation in deposition in different geological era, which is explained above. On comparing with Fig. 13, it can be concluded that basement depth in the extreme southern part of IGB is less as compared to northern part and near to floodplains along the river sites. Varying soil stiffness (V_s values) in vertical and horizontal direction of the IGB may be one of the reasons for past heavy damages due to earthquake anywhere in the IGB. So, understating of site-effects and liquefaction may be of prime importance to reduce seismic related losses.

7. Conclusion

In this study, a new correlation between V_s and SPT-N value has been derived by dividing the study area into Punjab-Haryana region, Uttar Pradesh region and Bihar region. Further the whole IGB has been seismically classified and average shear wave velocity map at shallow as well as deeper depths for the Indo-Gangetic Basin (IGB) has been developed. The least square, orthogonal and mixed effect approach have been used for determining the V_s and SPT-N correlation for PHR, UPR and BR. In this study both the corrected and uncorrected SPT-N value has been used for deriving V_s and SPT-N correlation. Variation of residuals with V_s have been studied for testing the performance of the

correlations derived using different regression approaches. Based on the analysis, it can be concluded that mixed effect relation is predicting better till $V_s \leq 250$ m/s in case of PHR and UPR, whereas the coefficient derived using least square analysis is predicting well in BR. However, in case of $V_s > 250$ m/s, the coefficient derived using orthogonal analysis is predicting well in all the three cases. For future work, it can be recommended that if less data is available, the V_s and SPT-N can be derived using orthogonal regression analysis instead of least square analysis. As till date no proper documentation is available for correcting SPT-N value with energy measurements in the study area, recently some research is started on understanding energy measurements and various corrections in SPT-N values by Indian Institute of Science. Therefore, uncorrected V_s and SPT-N is may be considered for any further analysis. V_{s30} in PHR, UPR and BR varies from 160 to 1251, 147–1136 and 153–1152 m/s respectively. However, the variation in V_{s300} in PHR, UPR and BR increased to 402–2462, 415–2800 and 445 to 2227 m/s. The low shear velocity has been observed in PHR and BR region even at deeper depths. The results of this study will be used in site response study and spatial variability of shear wave velocity analysis for entire stretch of Indo Gangetic Basin.

Supplementary data to this article can be found online at https://doi.org/10.1016/j.jappgeo.2019.02.011.

Acknowledgment

The authors are extremely grateful to two anonyms reviewers and editor for their valuable suggestions which helped in improving the manuscript. The authors thank the Science and Engineering Research Board (SERB) of the Department of Science and Technology (DST), India for funding the project titled “Measurement of shear wave velocity at deep soil sites and site response studies”, Ref: SERB/F/162/2015-2016. Authors also thanked to Geological Society of India for providing the Geological and Lithological map required for the study.

References

Akin, M.K., Kramer, S.L., Topal, T., 2011. Empirical correlations of shear wave velocity (Vs) and penetration resistance (SPT-N) for different soils in an earthquake-prone area (Erbaa-Turkey). Eng. Geol. 119, 1–17. https://doi.org/10.1016/j.enggeo.2011.01.007.

Anbazhagan, P., Sitharam, T.G., 2008. Mapping of average shear wave velocity for Bangalore region: a case study. J. Environ. Eng. Geophys. 13 (2), 69–84.

Anbazhagan, P., Parihar, A., Rashmi, H.N., 2012. Review of correlations between SPT N and shear modulus: a new correlation applicable to any region. Soil Dyn. Earthq. Eng. 36, 52–69.

Anbazhagan, P., Kumar, A., Sitharam, T.G., 2013. Pure Appl. Geophys. 170, 299. https://doi.org/10.1007/s00024-012-0525-1.

Anbazhagan, P., Bajaj, K., Reddy, G.R., Phanikanth, V.S., Yadav, D.N., 2016. Quantitative assessment of shear wave velocity correlations in the shallow bedrock sites. Indian Geotech. J. 46 (4), 381–397.

Andrus, R.D., Fairbanks, C.D., Zhang, J., Camp III, W.M., Casey, T.J., Cleary, T.J., Wright, W.B., 2006. Shear-wave velocity and seismic response of near-surface sediments in Charleston, South Carolina. Bull. Seismol. Soc. Am. 96, 1897–1914.

Bajaj, K., Anbazhagan, P., 2019. Spatial variability of shear wave velocity in the deep and active Indo-Gangetic Basin. Geophys. J. Int. (Under Review).

Bates, D.M., Maechler, M., Bolker, B., 2013. Lme4: Linear mixed-effect models using S4 classes R Manual. https://cran.r-project.org/web/packages/lme4/index.html, Accessed date: November 2016.

Bisaria, B.K., Pamdey, B.K., Khan, A.U., Bhartiya, S.P., 1996. Geomorphology and evaluation of Ganga plain in Uttar Pradesh. Geol. Surv. Spl. Pub. 21 (2), 209–214.

Burbank, D.W., 1992. Causes of recent Himalayan uplift deduced from deposited patterns in Ganga Basin. Nat. 357, 680–683.

Castellaro, S., Mulargia, F., Rossi, P.L., 2008. Vs30: proxy for seismic amplification? Seismol. Res. Lett. 79 (4), 540–543. https://doi.org/10.1785/gssrl.79.4.540.

Dikmen, Ü., 2009. Statistical correlations of shear wave velocity and penetration resistance for soils. J. Geophys. Eng. 6, 61–72. https://doi.org/10.1088/1742-2132/7/1/N02.

Foti, S., Comina, C., Boiero, D., Socco, L.V., 2009. Non-uniqueness in surface-wave inversion and consequences on seismic site response analyses. Soil Dyn. Earthq. Eng. 29, 982–993.

Foti, S., Parolai, S., Bergamo, P., Giulio, G.D., Maraschini, M., Milana, G., Picozzi, M., Puglia, R., 2011. Surface wave surveys for seismic site characterization of accelerometric stations in ITACA. Bull. Earthq. Eng. 9, 1797–1820.

Frankel, A.D., Carver, D.L., Williams, R.A., 2002. Nonlinear and linear site response and basin effects in Seattle for the M 6.8 Nisqually, Washington, earthquake. Bull. Seismol. Soc. Am. 92, 2,090–2,109.

Fujiwara, T., 1972. Estimation of Ground Movements in Actual Destructive Earthquakes. Proceedings of the Fourth European Symposium on Earthquake Engineering, London, pp. 125–132.

GSI (Geological Survey of India), 2006. Geological and Mineral Resources of the States of Haryana (Part- XVIII. Govt. of India. ISSN 0579-4706).

GSI (Geological Survey of India), 2012. Geological and Mineral Resources of the States of India Part XV: Punjab and Chandigarh Govt. of India. (ISSN 0579-4706).

Gunn, P.J., 1997. Application of aeromagnetic surveys to sedimentary basin studies. AGSO J. Aust. Geol. Geophys. 17, 133–144.

Hanumantharao, C., Ramana, G.V., 2008. Dynamic Soil properties for microzonation of Delhi, India. Journal of Earth System Science 117 (S2), 719–730.

Hasançebi, N., Ulusay, R., 2007. Empirical correlations between shear wave velocity and penetration resistance for ground shaking assessments. Bull. Eng. Geol. Environ. 66, 203–213.

Hough, S.E., Bilham, R., 2008. Site response of the Ganges basin inferred from re-evaluated macroseismic observations from the 1897 Shillong, 1905 Kangra, and 1934 Nepal earthquakes. J. Earth Syst. Sci. 117, 773–782.

Imai, T., Tonouchi, K., 1982. Correlation of N-value with S-wave velocity and shear modulus. Proceedings of the 2nd European Symposium of Penetration Testing, Amsterdam, pp. 57–72.

Ismail, A., Denny, F.B., Metwaly, M., 2014. Comparing continuous profiles from MASW and shear-wave reflection seismic methods. J. Appl. Geophys. 105, 67–77.

Jafari, M.K., Asghari, A., Rahmani, I., 1997. Empirical correlation between shear wave velocity and SPT-N values for south of Tehran soils. Proceedings of the 4th Int. Conf. On Civil Engineering, (Tehran, Iran) (in Persian).

Karabulut, S., 2018a. a. Soil classification for seismic site effect using MASW and ReMi methods: a case study from western Anatolia (Dikiliizmir). J. Appl. Geophys. 150, 254–266.

Karabulut, S., 2018b. b. A Novel urban transformation criteria from a Geosciences perspective: as case study in Bursa, NW Turkey. J. Clean. Prod. 195, 1437–1456.

Kiku, H., Yoshida, N., Yasuda, S., Irisawa, T., Nakazawa, H., Shimizu, Y., Ansal, A., Erkan, A., 2001. In-situ penetration tests and soil profiling in Adapazari, Turkey. Proceedings of the ICSMGE/TC4 Satellite Conference on Lessons Learned From Recent Strong Earthquakes, pp. 259–265.

Kumar, S., Parkash, B., Manchanda, M.L., Singhvi, A.K., 1996. Holocene landform and soil evolution of the western Gangetic Plains: implications of neotectonics and climate. Zeit. Geomorph. N.F. Suppl.-Bd. 103, 283–312.

Kuo, C.H., Wen, K.L., Hsieh, H.H., Lin, C.M., Chang, T.M., Kuo, K.W., 2012. Site classification and Vs30 estimation of free-field TSMIP stations using the logging data of EGDT. Eng. Geol. 129–130, 68–75. https://doi.org/10.1016/j.enggeo.2012.01.013.

Lee, V.W., Trifunac, M.D., 2010. Should average shear-wave velocity in the top 30 m of soil be used to describe seismic amplification? Soil Dyn. Earthq. Eng. 30 (11), 1540–1549.

Lin, C., Lin, C., Chien, C., 2017. Dispersion analysis of surface wave testing-SASW vs. MASW. J. Appl. Geophys. 143, 223–230.

Lyon-Caen, H., Molnar, P., 1985. Gravity anomalies, flexure of the Indian Plate, and the structure, support and evolution of the Himalaya and Ganga Basin. Tectonics 4, 513–538.

Mahajan, A.K., Sporry, R.J., Champati ray P.K., Ranjan R.R., Slob S., Van W.S., 2007. Methodology for site-response studies using multi-channel analysis of surface wave technique in Dehradun city, Curr. Sci. 92 (7), 945–955.

Mahajan, A.K., Mundepi, A.K., Chauhan, N., et al., 2012. Active seismic and passive micrometer HVSR for assessing site effects in Jammu city, NW Himalaya, India-a case study. J. Appl. Geophys. 77, 51–62.

Maheshwari, U., Boominathan, R.A., Dodagoudar, G.R., 2010. Seismic site classification and site period mapping of Chennai city using geophysical and geotechnical data. J. Appl. Geophys. 72, 152–168.

Malekmohammadi, M., Pezeshk, S., 2015. Ground motion site amplification factors for sites located within the Mississippi embayment with consideration of Deep Soil Deposits. Earthquake Spectra 31 (2), 699–722.

Mayne, P.W., Coop, M.R., Springman, S.M., Huang, A.B., Zornberg, J.G., 2009. Geomaterial behavior and testing (Comportement et essai de Geomaterial). Proc. 17th Intl. Conf. Soil Mechanics & Geotechnical Engineering, Alexandria, Egypt, pp. 2777–2872.

Mucciarelli, M., Gallipoli, M.R., 2006. Comparison between Vs30 and other estimates of site amplifcation in Italy. First European Conference on Earthquake Engineering and Seismology, a joint event of the 13th European Conference on Earthquake Engineering and 30th General Assembly of the European Seismological Commission, Geneva, Switzerland, 3–8 Sept., paper no. 270.

Naik, S.P., Patra, N.R., Malik, J.N., 2014. Geotech. Geol. Eng. 32, 131. https://doi.org/10.1007/s10706-013-9698-3.

Ohta, Y., Goto, N., 1978. Empirical shear wave velocity equations in terms of characteristic soil indexes, Earthquake Eng. Struct. Dynam. 6 (2), 167–187.

Okada, H., 2003. The microtremor survey method. Geophysical Monographs Series, no. 12. Society of Exploration Geophysicists.

Orubu, A., Khalil, M.A., Rutherford, B., Shaw, G., Gebril, A., Carsarphen, C., 2018. Geophysical investigation of dewatering in Lolo Creek, Southwest Missoula, Montana, USA. J. Appl. Geophys. 155, 149–161 (in press).

Park, D., Hashash, Y.M.A., 2004. Probabilistic seismic hazard analysis with nonlinear site effects in the Mississippi embayment. Proceedings of the 13th World Conference on Earthquake Engineering, Vancouver, CD-Rom edition, paper no. 1549.

Park, C., Miller, R., 2008. Roadside passive multichannel analysis of surface waves (MASW). J. Environ. Eng. Geophys. 13, 1–11.

Park, C., Miller, R., Xia, J., 1998. Imaging dispersion curves of surface waves on multichannel record. Soc. Explor. Geophys. Expand. Abstr. 1377–1380.

Park, C.B., Miller, R.D., Ryden, N., Xia, J., Ivanov, J., 2005. Combined use of active and passive sur-face waves. J. Environ. Eng. Geophys. 10 (3), 323–334.

Park, C.B., Miller, R.D., Xia, J., Ivanov, J., 2007. Multichannel analysis of surface waves (MASW)-active and passive methods. Lead. Edge 26, 60–64.

Pati, P., Pradhan, R.M., Dash, C., et al., 2015. Terminal fans and the Ganga plain tectonism: a study of neotectonism and segmentation episodes of the Indo-Gangetic foreland basin, India. Earth-Sci Rev. 148, 134–149.
Pitilakis, K., Raptakis, D., Lontzetidis, K.T., Vassilikou, T., Jongmans, D., 1999. Geotechnical and geophysical description of Euro-Seistests, using field and laboratory tests, and moderate strong ground motions. J. Earthq. Eng. 3, 381–409.
Prakash, Om, Sinha, A.P., Verma, N.P., Reddy, B.S.S., 1990. Quaternary geological and geomorphologival mapping of the Ganga–Sone alluvial belt in Aurangabad, Bhojpur, Jehanabad, Patna and Rohtas districts, Bihar. Rec. Geol. Surv. India 123 (3) 8p.
Raef, A., Gad, S., Tucker-Kulesza, S., 2015. Multichannel analysis of surface waves and investigation of downhole acoustic televiewer imaging, ultrasonic Vs and Vp, and vertical seismic profiling in an NEHRP-standard classification, South of Concordia, Kansas, USA. J. Appl. Geophys. 121, 149–161.
Rahman, M.Z., Siddiqua, S., Kamal, A.S.M.M., 2016. Shear wave velocity estimation of the near-surface materials of Chittagong City, Bangladesh for seismic site characterization. J. Appl. Geophys. 134, 210–225.
Rao, M.B.R., 1973. The subsurface geology of the indo-gangetic plains. Geol. Soc. India 14, 217–242.
Sahu, S., Saha, D., Dayal, S., 2015. Sone megafan: a non-Himalayan megafan of craton origin on the southern margin of the middle Ganga Basin, India. Geomorphology 250, 349–369.
Saini, H.S., Anand, V.K., 1996. Lithostratigraphy framework and sedimentological evolution of the Quaternary deposits of northwestern Haryana. Gel. Surv. India Spl. Pub. 21 (2), 227–231.
Sastri, V.V., Bhandari, L.L., Raju, A.T.R., Dutta, A.K., 1971. Tectonic framework and subsurface stratigraphy of the Ganga Basin. J. Geol. Soc. India 12, 222–233.
Satyam, N.D., Rao, K.S., 2008. Seismic site characterization in Delhi region using multichannel analysis of shear wave velocity (MASW) testing. Electron. J. Geotech. Eng. 13, 167–183.
Seed, H.B., Idriss, I.M., Arango, I., 1981. Evaluation of liquefaction potential using field performance data. J. Geotech. Eng. ASCE 109, 458–482.
Singh, I.B., 1996. Geological evolution of Ganga plain – an overview. J. Paleont. Soc. India 41, 99–137.
Singh, I.B., Singh, M., 1992. The Ganga river valley: Alluvial valley in active foreland basin. 29th Int. Geol. Cong. Kyoto, Japan.
Socco, L.V., Foti, S., Boiero, D., 2010. Surface-wave analysis for building near-surface velocity models: established approaches and new perspectives. Geophysics 75. https://doi.org/10.1190/1.3479491(75A83–75A102).
Srinagesh, D., Singh, S.K., Chadha, R.K., Paul, G., et al., 2011. Amplification of seismic waves in the central Indo-Gangetic Basin. India. Bull. Seismol. Soc. Am. 101, 2231–2242.
Stafford, P.J., 2014. Crossed and nested mixed-effects approaches for enhanced model development and removal of the ergodic assumption in empirical ground-motion models. Bull. Seismol. Soc. Am. 104, 702–719.
Wald, L.A., Mori, J., 2000. Evaluation of methods for estimating linear site-response amplifcations in the Los Angeles region. Bull. Seismol. Soc. Am. 90, S32S42.
Xia, J., Miller, R.D., Park, C.B., 1999. Estimation of near-surface shear-wave velocity by inversion of Rayleigh waves. Geophysics 64, 691–700.